Coordination Chemistry Reviews, 60 (1984) 1–66
Elsevier Science Publishers B.V., Amsterdam – Printed in The Netherlands

BIOINORGANIC APPLICATIONS OF MAGNETIC CIRCULAR DICHROISM SPECTROSCOPY: COPPER, RARE-EARTH IONS, COBALT AND NON-HEME IRON SYSTEMS

DAVID M. DOOLEY

Department of Chemistry, Amherst College, Amherst, MA 01002 (U.S.A.)

JOHN H. DAWSON

Department of Chemistry, University of South Carolina, Columbia, SC 29208 (U.S.A.)

(Received 26 September 1983)

CONTENTS

0010-8545/84/$19.80

A. INTRODUCTION

Understanding the correlation between structure and function has long been at the heart of many of the investigations undertaken by chemists and biochemists. Because all molecules interact with light in characteristic and diagnostic ways, the use of various spectroscopic techniques is often the method of choice for determining the electronic structure and the physical structure of molecules. Bioinorganic systems, especially metalloproteins, are often rich in chromophoric constituents and are therefore particularly amenable to spectroscopic examination. Indeed, the armamentarium of the bioinorganic spectroscopist includes ultraviolet–visible, infrared, and X-ray absorption; *X*-ray photoelectron; resonance Raman; Mössbauer; electron paramagnetic, nuclear magnetic and electron-nuclear double resonance; and circular and magnetic circular dichroism (CD, MCD) spectroscopy. This review article will focus on applications of MCD spectroscopy; for reasons to be outlined below, this technique has particular advantages for studying bioinorganic systems. However, it should be obvious that no single technique, not even X-ray diffraction, will provide the investigator with all the information desired about the electronic and physical structures of the system under study. Such information includes the oxidation state, spin state, and magnetic properties of the metal; the identity of the ligands present; the geometry of the metal–ligand structure; the number of ligands and the metal–ligand bond distances. Numerous examples will be discussed on the use of MCD spectroscopy to determine all but the last one of the physical parameters listed above.

MCD is the difference in absorption of left and right circularly polarized light induced by an external, longitudinal (parallel to the direction of light propagation) magnetic field. It is therefore a type of Zeeman experiment where the magnetic field splits or mixes the zero field energy levels. When the Zeeman splitting is directly resolvable, MCD provides no additional information compared to a conventional Zeeman experiment with circularly polarized light. Most bioinorganic systems display broad electronic absorption bands which make Zeeman splittings undetectable, so the great utility of MCD lies in its extension of the Zeeman experiment to broad absorption bands. Thus MCD can be used to assign bands to particular transitions, characterize ground- and excited-state symmetries and angular momenta, measure intra- and intermolecular interactions, and can form a basis for structural comparisons. The sensitivity of MCD to changes in molecular structure, although not always well understood in theory, provides a useful empirical tool for structure determination.

Although natural circular dichroism and MCD are revealed in the same physical property (i.e., a difference in the extinction coefficients for left and

right circularly polarized light), the origin of these effects is different. Inherent structural dissymmetries either in the chromophore itself or in the environment in which the chromophore is located give rise to CD effects whereas MCD results from the direct effect of a magnetic field on degenerate and near-degenerate electronic energy levels. Because CD and MCD can be both negative and positive, their spectra show considerably more fine structure than seen in corresponding absorption spectra. Thus, for empirical comparisons, they yield twice as much information (i.e., sign and intensity) as a function of wavelength, than does absolute absorption spectroscopy and therefore have more "fingerprinting" capability. However, because of its origin, CD is very sensitive to the details of the microenvironment whereas MCD is induced by the effect of the external magnetic fields on the electronic structure of the molecule. Thus, MCD is more sensitive to changes in the electronic structure which, in turn, reflect changes in physical structure. This relative insensitivity of MCD to environmental factors allows direct comparisons to be made between model metal complexes in organic solvents and protein bound metal sites. In comparison to EPR, MCD has the advantage that it need not be measured at cryogenic temperatures as is often necessary for EPR studies and it is applicable to all oxidation states. Low temperature MCD studies are quite feasible and provide additional and very useful information, as will be discussed. Finally, the concentrations necessary for MCD studies are the same as are needed for optical absorption spectroscopy. For typical bioinorganic systems this means 10–1000 μM.

This article focuses on the application of MCD spectroscopy to some systems of interest to the bioinorganic chemist. After a brief discussion of the theory of MCD spectroscopy, we will review the use of this technique in studying copper proteins, rare-earth ion and cobalt substituted proteins and non-heme iron proteins. Except for the cobalt section where alternative recent review articles are available, we have attempted to be quite thorough in our coverage of the literature. As MCD spectroscopy has been more extensively applied to the study of heme proteins, a review of that topic will be deferred for the future.

B. THEORY

Many excellent discussions of the theory of MCD are available, ranging from elementary to quite sophisticated [1–14]. It is not our intention to present yet another summary, but rather to provide the reader with sufficient theoretical background to follow the subsequent discussions of experimental results, and to provide a guide to other, more complete, treatments of the theory. In most instances the nature of the problem will provide a reliable guide to the level of theory necessary in order to interpret the data.

Generally much more detailed information is obtainable from systems of accurately known structure and relatively high symmetry; group theory and ligand field theory (including the formalism and application of irreducible tensor methods) at a level unfamiliar to most chemists are required in order to extract all the information from MCD experiments on such systems. Most biological chromophores possess only low symmetry and many have uncertain structures, so familiarity with advanced theoretical concepts is often unnecessary. MCD spectra can still provide qualitative, and in favorable cases, quantitative electronic structural information in these circumstances. Additionally, MCD experiments can be helpful in elucidating structural features, e.g. identifying transition metal-ion ligands and coordination geometries in metalloproteins. In order to critically evaluate any MCD experiment, some knowledge of the theory is essential, as we hope becomes apparent in this section and in our review of experimental results.

A circularly polarized photon has, in addition to an energy, parity, and angular momentum, a well-defined z component of angular momentum, M_J. For left circularly polarized light $M_J = +1$ and for right circularly polarized light $M_J = -1$. This leads immediately to the selection rules for absorption of left and right circularly polarized light, $\Delta M_J = +1$ and $\Delta M_J = -1$, respectively. The total MCD can be described as the sum of three terms, A, B and C. Simple demonstrations of the electronic factors responsible for A and C terms have been given several times in the literature for the case of an isolated electronic transition (as in a single atom). It should be noted that some of the earlier discussions are slightly erroneous [5,6] and the reader is referred to ref. 15 for the corrections.

Extending MCD theory to molecules with broad absorption bands, composed of many overlapping vibronic transitions, is not trivial, but is clearly of most interest to chemists. Fortunately the theory has been substantially worked out and is well described in the literature [1–6,8,11]. The two major theoretical approaches are: the "Rigid Shift" (RS) approximation which assumes that the overall band-shape does not change as a result of the Zeeman shift; and the method of moments in which parameters identical to those that occur in the RS approximation are obtained from a moment analysis of the observed bands. Here we will consider the RS approach, which was developed first and follows most directly from the theory for discrete lines. Subsequently the limitations of the RS approximation will be considered and briefly compared to the advantages and limitations of moment analysis.

Lucid derivations of the MCD dispersion equations are available elsewhere [1–6]. We will briefly summarize the procedure here in order to provide some additional background to our discussion of the equations that follow. Generally a semi-classical description of absorption is adopted (that is, a

quantum mechanical treatment of the molecule is combined with a classical picture of light), and the external magnetic field effects (Zeeman energies, field-induced mixing of zero-field states, and the electric dipole matrix elements) are calculated via perturbation theory. Wavefunctions are chosen within the Born–Oppenheimer approximation to diagonalize the z-component (parallel to the light propagation direction) of the magnetic dipole moment operator. Further, population changes must be accounted for if any ground state degeneracy exists that is lifted by the external field. Finally, the MCD lineshape is usually approximated as a Taylor series expansion about the zero-field absorption line. When all is said and done we obtain, for the transition $A \rightarrow J$, the RS MCD dispersion (ΔA, the difference in absorption of left and right circularly polarized light) given in

$$\Delta A(A \rightarrow J) = \gamma\left\{-A_1\left(\frac{\partial f}{\partial E}\right) + \left(B_0 + \frac{C_0}{kT}\right) f\right\} \beta H b l \tag{1}$$

$$\gamma = \frac{N\pi^2\alpha^2 \log e}{250\hbar c n}\,; \int_0^\infty \frac{f(E_{JA}, E)}{E}\,\mathrm{d}E = 1$$

where N = Avogadro's number, b = concentration in mol l^{-1}, l = pathlength (cm), β is the Bohr magneton, c is the speed of light, n is the refractive index and H the magnitude of the magnetic field. The electric field, $\bar{e}$, at the absorbing center is proportional to the macroscopic $\bar{E}$ of the light as follows: $\bar{e} = \alpha\bar{E}$. $f(E_{JA}, E)$ is the lineshape (gaussian, for example) of the transition and it is a function of both the transition energy, $E_{JA} = E_J - E_A$, and the incident photon energy, E.

It is clear from eqn. (1) that, in principle, the MCD dispersion is composed of three terms, $-A_1(\partial f/\partial E)$, $B_0 f$ and $C_0 f/kT$, called the A, B and C terms, respectively. The term $-A_1(\partial f/\partial E)$ in eqn. (1) obviously will give rise to a derivative shaped dispersion in an MCD spectrum that is characteristic of an A term. Positive A terms have negative lobes at lower energy and positive ones at higher energy (Fig. 1). B and C terms display lineshapes similar to a zero-field absorption band, except for the possibility of both positive and negative sign in MCD bands. A_1, B_0, and C_0 are parameters that depend on the electric dipole selection rules for the absorption of circularly polarized light in a magnetic field. They are given explicitly for light propagating parallel to the z direction in eqn. (2).

$$A_1 = +\frac{1}{d_A}\sum_{\alpha,\lambda}\left[|\langle A_\alpha|m_-|J_\lambda\rangle|^2 - |\langle A_\alpha|m_+|J_\lambda\rangle|^2\right]$$

$$\times\left[\langle J_\lambda|L_z + 2S_z|J_\lambda\rangle - \langle A_\alpha|L_z + 2S_z|A_\alpha\rangle\right] \tag{2a}$$

$$B_0 = \frac{-2}{d_A} \sum_{\alpha,\lambda} Re \Bigg\{ \sum_{K_\kappa \neq J} [\langle A_\alpha | m_- | J_\lambda \rangle \langle K_\kappa | m_+ | A_\alpha \rangle |$$

$$- \langle A_\alpha | m_+ | J_\lambda \rangle \langle K_\kappa | m_- | A_\alpha \rangle] \frac{\langle J_\lambda | L_z + 2S_z | K_\kappa \rangle}{W_K - W_J}$$

$$+ \sum_{K_\kappa \neq A} [\langle A_\alpha | m_- | J_\lambda \rangle \langle J_\lambda | m_+ | K_\kappa \rangle$$

$$- \langle A_\alpha | m_+ | J_\lambda \rangle \langle J_\lambda | m_- | K_\kappa \rangle] \frac{\langle K_\kappa | L_z + 2S_z | A_\alpha \rangle}{W_K - W_A} \Bigg\} \tag{2b}$$

$$C_0 = -\frac{1}{d_A} \sum_{\alpha,\lambda} \left[|\langle A_\alpha | m_- | J_\lambda \rangle|^2 - |\langle A_\alpha | m_+ | J_\lambda \rangle|^2 \right] \langle A_\alpha | L_z + 2S_z | A_\alpha \rangle \tag{2c}$$

A_α and J_λ are the ground and excited electronic states, respectively, with components α and λ; K_κ is any other state that can be mixed with A_α or J_λ when $H \neq 0$; d_A is the degeneracy of the state A_α, $m_\pm = [1/\sqrt{2}](m_X \pm i m_Y)$ is the electric dipole moment operator, and $\mu_Z = -\beta(L_z + 2S_z)$ is the z component of the magnetic-dipole operator. In eqn. (2), only the interaction between the electrons and $m_\pm$ is considered (the nuclear part has been factored out via the Franck–Condon approximation) and the matrix elements are evaluated at the equilibrium nuclear configuration, R_0. The electronic energy differences between states, e.g. $\Delta W = W_K - W_J$, are also evaluated at R_0.

These formidable appearing expressions are easier to analyze if we note that matrix elements like $\langle A_\alpha | m_\pm | J_\lambda \rangle$ appear in the equations for A_1 and C_0. Now the zero-field absorption oscillator strength (D_0) for the $A \rightarrow J$ transition is defined by eqn. (3).

$$D_0(A \rightarrow J) = \frac{1}{2d_A} \sum_{\alpha,\lambda} \left[|\langle A_\alpha | m_+ | J_\lambda \rangle|^2 + |\langle A_\alpha | m_- | J_\lambda \rangle|^2 \right] \tag{3}$$

Therefore when the ratios A_1/D_0 and C_0/D_0 are taken, the $\langle A_\alpha | m_\pm | J_\lambda \rangle$ matrix elements will often cancel out, within a proportionality factor, and thus the electric-dipole matrix elements do not have to be calculated directly (which is difficult to do). Further, D_0 may be experimentally determined from the integrated intensity of the zero field absorption. We finally obtain

$$\frac{A_1}{D_0} \sim \sum_{\alpha,\lambda} \langle J_\lambda | L_z + 2S_z | J_\lambda \rangle - \langle A_\alpha | L_z + 2S_z | A_\alpha \rangle$$

$$\frac{C_0}{D_0} \sim -\sum_{\alpha} \langle A_\alpha | L_z + 2S_z | A_\alpha \rangle \tag{4}$$

It is evident that A terms arise only when the matrix elements of either the ground or excited state with the magnetic dipole moment operator are non-zero. C terms appear only when the matrix element of the ground state with this operator is non-zero. Since only degenerate states will have non-zero magnetic dipole matrix elements, it follows that A terms are possible only when the ground and/or excited states are degenerate and C terms exist only

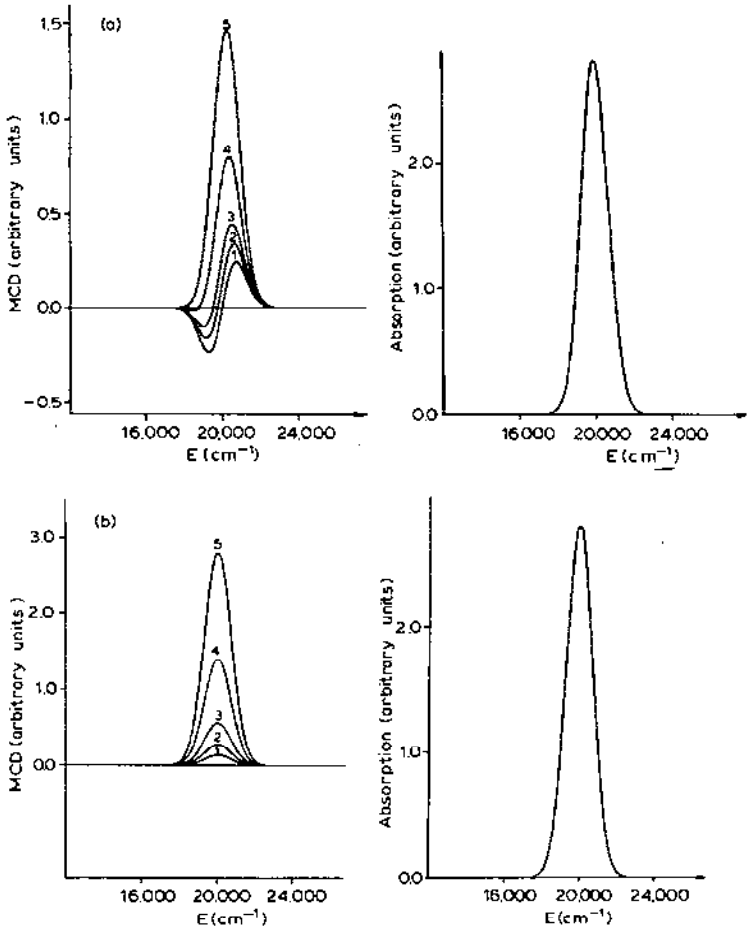

Fig. 1. Magnetic circular dichroism dispersion according to the rigid shift model. In (a) the effect of varying the relative magnitudes of the A and $(B + C)$ terms is illustrated. The zero-field absorption is calculated for a bandshape function, $f = \Delta^{-1}\ \pi^{-1}\ \exp[-(E - E^\circ)^2/\Delta^2]$, $E^\circ = 20000\ \text{cm}^{-1}$, $\Delta = 1000\ \text{cm}^{-1}$. The MCD is calculated from eqn. (1) with $A_1 = 1$, $\beta H = 1\ \text{cm}^{-1}$ and $(B_0 + C_0/kT)$ equal to: (1) 0; (2) 5×10^{-4}; (3) 1×10^{-3}; (4) 2.5×10^{-3}; (5) 5×10^{-3}. In (b) the effect of varying the temperature (T) on the C terms is illustrated. The zero-field absorption is identical to (a). The MCD is calculated with $A_1 = B_0 = 0$, $C_0 = 1$ and kT equal to: (1) 200 cm^{-1}; (2) 100 cm^{-1}; (3) 50 cm^{-1}; (4) 20 cm^{-1}; (5) 10 cm^{-1}. Adapted from ref. 3.

if the ground state is degenerate. A non-zero A term in the absence of ground state degeneracy ($C_0 = 0$) proves excited state degeneracy, and a non-zero C term establishes that the ground state is degenerate. When only the ground state is degenerate, $A_1 = C_0$. If both the ground and excited states are degenerate then $A_1 \neq C_0$. Inspection of eqn. (2a) shows that the excited state and ground state Zeeman interactions contribute to A_1 in this case. In many systems of interest both orbital and spin degeneraccy are possible. Note that the expressions for A_1 and C_0 in eqn. (2) contain the term $|\langle A_\alpha|m_-|J_\lambda\rangle|^2 - |\langle A_\alpha|m_+|J_\lambda\rangle|^2$. These electric dipole matrix elements are independent of spin when spin–orbit coupling is zero. In this limit only orbital degeneracy contributes to A_1 and C_0. To a first approximation the MCD of spin-allowed transitions will still be independent of spin when the spin–orbit splittings are non-zero but much less than the bandwidth and kT [13]. An important exception occurs for transitions from a spin-degenerate but orbitally non-degenerate ground state to the spin–orbit split components of an orbitally degenerate excited state [13]. In this case the C terms do not cancel (vide infra). Examples of these effects will be encountered later in this review. Although spin–orbit coupling is often only a minor influence on the zero-field absorption it can have profound effects on the MCD.

In favorable cases, both the magnitude and sign of the ground state g value can be obtained from analysis of C terms, and the excited state g value (magnitude and sign) can be obtained from the A_1 value. More generally, both the sign and magnitude of A and C terms will depend on state symmetries, magnetic moments and the selection rules for circularly polarized light. The information content of A and C terms is therefore great.

So far little has been said about the interpretation of B terms, and as we shall see, for good reason. Referring to eqn. (2), it is evident that B_0 depends on matrix elements among the ground state and/or excited state of interest and all other possible excited states, including the continuum. Clearly such a summation is impractical, and in order to evaluate B terms, truncating the summation is necessary. The usual approach is to argue that only states relatively close in energy need to be considered, owing to the ΔW^{-1} term in the expression for B_0. Only if the field-induced matrix element products like $\langle J_\lambda|L_z + 2S_z|K_\kappa\rangle\langle K_\kappa|m_-|A_\alpha\rangle$ are small relative to the corresponding energy separation, $W_K - W_J$, will this approximation be valid; it is difficult to tell in practice if this is likely. While it is true that in order for B_0 to be non-zero, electric dipole and magnetic dipole matrix elements between two states, i.e. $\langle K_\kappa|m_\pm|A_\alpha\rangle$ and $\langle J_\lambda|L_z + 2S_z|K_\kappa\rangle$, must exist simultaneously, this requirement is not very restrictive in practice given the large number of possible excited states. Nevertheless some success in using B terms to assign electronic transitions has been reported; B terms have also proven useful as a basis for empirical correlations and for comparing the electronic structures

of a series of related compounds (see refs. 16–21 for some examples). In most biological systems of interest to the inorganic chemist, B terms can be expected to be present, although as the following discussion indicates, they may be small relative to A and especially C terms, particularly at low temperatures.

A, B and C terms may be distinguished via their dispersion and temperature dependence. As eqn. (1) indicates, the terms are additive so an MCD spectrum may be composed of all three. Following Stephens [3], we can write

$$\left(\frac{\partial f}{\partial E}\right)_{\max} \cong \frac{(f)}{\Gamma}\max \tag{5}$$

where Γ is the linewidth of f. C terms are proportional to $(kT)^{-1}$. Thus, we can express the maximum contributions of A, B and C terms to ΔA.

$$A\colon B\colon C\colon \cong \Gamma^{-1}\colon \Delta W^{-1}\colon (kT)^{-1} \tag{6}$$

For example, at room temperature, we might have $\Gamma = 10^3$ cm^{-1}, $\Delta W = 10^4$ cm^{-1} and $kT = 200$ cm^{-1} leading to the following relative intensity pattern [3].

$$A\colon B\colon C\colon \cong 10\colon 1\colon 50 \tag{7}$$

Clearly, the relative intensities will change drastically as T decreases and C terms are thus easily identified. Some care is necessary, however, because Γ may also be temperature dependent (many bands sharpen upon cooling), so A terms may also depend on temperature, although not as $(T)^{-1}$. For this reason measurement of the absorption spectrum at temperatures where the MCD is recorded is a necessity.

A terms may often be identified by their characteristic dispersion; the derivative-shaped curve with a cross-over (zero) point at the energy of the zero-field absorption maximum. Derivative-shaped bands can appear in an MCD spectrum even if $A_1 = 0$, however. Suppose two excited states J^1 and J^2, separated in energy by $\Delta W_{J^2J^1}$ are non-degenerate. If the C terms for the $A \rightarrow J^1, J^2$ transitions are opposite in sign ($C_0^1 = -C_0^2$) and $\Delta W_{J^2J^1}$ is much smaller than the bandwidth, then ΔA from the C terms is given in [3]

$$\Delta A = \gamma C_0^2 \Delta W_{J^2J^1}\left(\frac{-\partial f_1}{\partial E}\right)(\beta H/kT)bl \tag{8}$$

This will give rise to a derivative-shaped dispersion, a "pseudo-A" term, with a magnitude proportional to $\Delta W_{J^2J^1}$ but the excited states involved are not degenerate. Spin–orbit splitting of an excited state, where J^2 and J^1 are different spin–orbit components, can result in a pseudo-A term that is composed of oppositely signed C terms. Pseudo-A terms can also result from

overlapping transitions with oppositely signed B_0 parameters. Careful variable temperature measurements are necessary to sort out the possibilities. In conclusion, measurement of both MCD and zero-field absorption at several temperatures over as wide a range as possible, in conjunction with a knowledge of the system and theoretical calculations of expected signs and rough magnitudes, occasionally is necessary in order for the contributions of A, B and C terms to be separated.

All of the expressions considered to this point assume that kT is much greater than the Zeeman energy. If not, linearity in H is lost and different equations must be used that explicitly include Boltzmann factors for the ground state Zeeman levels, as in

$$\Delta A = \gamma \left(\sum_{\alpha,\lambda} \frac{\exp(\langle A_\alpha|\mu_z|A_\alpha\rangle H/kT)}{\sum_\alpha \exp(\langle A_\alpha|\mu_z|A_\alpha\rangle H/kT)} \times \left[|\langle A_\alpha|m_-|J_\lambda\rangle|^2 - |\langle A_\alpha|m_+|J_\lambda\rangle|^2 \right] f \right) bl \tag{9}$$

As H/T increases, population changes will occur until the Zeeman energy becomes very much greater than kT, at which point no further population change is possible and the system is saturated (Fig. 2). An illustrative and important example is the saturation behavior played by a ground state Kramer's doublet (as in Cu(II) complexes). In this case we have

$$-\langle A_\alpha|\mu_z|A_\alpha\rangle = g\beta H M_\alpha \begin{pmatrix} M_1 = -1/2 \\ M_2 = +1/2 \end{pmatrix} \tag{10}$$

Calculating the MCD dispersion from eqns. (9) and (10) as a function of temperature yields [3]

$$\Delta A = \gamma \tanh\left(\frac{g\beta H}{2kT}\right)\left[\sum_\lambda \left[|\langle A_{\alpha_1}|m_-|J_\lambda\rangle|^2 - |\langle A_{\alpha_1}|m_+|J_\lambda\rangle|^2 \right]\right] \quad \alpha_1 \equiv M_1 \tag{11}$$

Note that the electric dipole matrix elements are constant for a specified $A \rightarrow J$ transition and are temperature independent, thus ΔA depends on H and T as $\tanh(g\beta H/2kT)$, as shown in Fig. 2. We see that the saturation curve is determined by only the ground state g value. Equation (11) is appropriate for an isotropic system; the theory has been derived for axial and rhombic systems as well [22]. Another type of saturation may be observed when a non-degenerate state J lies very near the ground state A and when mixing of A and J is permitted by $H \neq 0$. When $E_J - E_A$ is small

compared to $\Gamma_{J\to K}$ and $\Gamma_{A\to K}$ for transitions to a higher energy excited state K then a contribution to ΔA of the following form will result

$$\Delta A \sim \tanh[(E_J - E_A)/2kT] \tag{12}$$

This "temperature dependent B term" will saturate at $kT \sim E_J - E_A$ and thus can be distinguished from the saturation behavior described by eqn. (11). Saturation curves can be very informative, providing, for instance, detailed information about ground state energies and zero-field degeneracies as well as any magnetic coupling. MCD is also non-linear with respect to H if the Zeeman splitting is large compared to the linewidth. Under these conditions C terms, if present, will not be linear in $(kT)^{-1}$. These effects are easily distinguished from saturation.

Some constraints on eqn. (2) should be noted. Most fundamental is the assumption that the "Rigid Shift" approximation is valid. This approximation and its difficulties have been fully discussed elsewhere [1–6]. The most important assumptions of the RS model are that the Born–Oppenheimer and Franck–Condon approximations hold simultaneously. In many instances this will not be true, although the breakdown in the approximations is often not sufficiently severe to discredit the results of analyses based on the RS approach. The most serious problem is the breakdown of the Born–Oppenheimer approximation when the Jahn–Teller effect is not zero. For non-degenerate states and Kramer's doublets, where the Jahn–Teller effect is exactly zero, the breakdown is not a problem. Furthermore, the optimistic (naive?) approach of ignoring the Jahn–Teller effect is often quite successful. Another approach, based on moment analysis, is described in

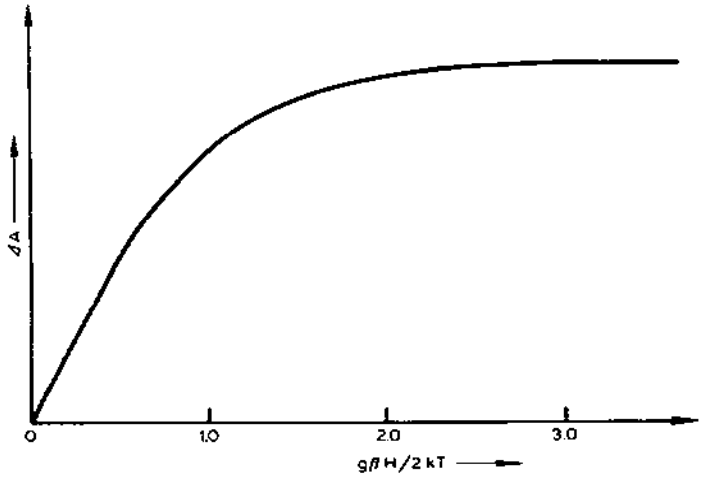

Fig. 2. MCD saturation curve for a system with a Kramer's doublet ground state. From ref. 3.

detail in the literature [3,4,6,8]. Moment analysis is considerably more rigorous than the RS approximation. The same parameters appear and are interpreted in much the same way as indicated here. The application and limitations of the method of moments have been well reviewed [3,4,6,8]. Some pertinent features are: (1) moments may only be calculated for isolated bands (absorbance equal to zero on either side); (2) in the case of overlapping transitions, sums of the parameters are obtained, e.g. $A_1^1 + A_1^2$ for overlapping $A \rightarrow J^1$ and $A \rightarrow J^2$ transitions; (3) the difficulties with the Jahn–Teller effect and Born–Oppenheimer breakdown in the RS approach are circumvented by moment analysis. It should also be noted that eqns. (1) and (2) strictly apply to localized electronic transitions of dilute, rigid centers. For rigid centers that are randomly oriented in physically identical sites (or in sites sufficiently similar that the orientation dependence is negligible), formally identical results are obtained. For solutions containing molecules that are free to move, it is necessary to assume a magnetically isotropic ground state. Usually the assumption is made that fluid molecular solutions can be treated as randomly oriented identical rigid centers. For a complete treatment, the reader is referred to a paper by Stephens [23]. A final consideration: the treatment presented here is appropriate for allowed electronic transitions. Both the RS approximation and moment analysis can be extended to the case of vibronically allowed transitions (intensity equal to zero in the Franck–Condon approximation) but the theory is considerably more complex.

We conclude this section with a brief description of where to go for more complete presentations of the theory. Our discussion borrowed heavily from three reviews by Stephens [1–3]. Reference 3 is particularly recommended as the most cogent and readable account of MCD theory at an intermediate level; it also includes several illustrative examples. Another excellent general review is that by Schatz and McCaffery [6]. For a basic introduction, the article by McCaffery [7] should be consulted, as well as some recent general reviews [9–12]. These latter reviews also include some very helpful practical sections on, among other things, data reduction, units, and instrumentation. At a more sophisticated level, the application of irreducible tensor methods to the MCD of high symmetry systems has been described [4,14]. Several informative applications, including bioinorganic examples, have recently been reviewed [8–12].

(i) Units

Unfortunately MCD has been reported in a wide variety of units, as will be evident from the figures reproduced in this review. The differential molar extinction coefficient per unit field, $\Delta\epsilon_M$, is now more or less generally

accepted for expressing MCD quantitatively. It is defined as

$$\Delta\epsilon_M(M^{-1}cm^{-1}T^{-1}) = \Delta\epsilon/H = \Delta A/blH$$

where $\Delta\epsilon = \epsilon_L - \epsilon_R$ and $\Delta A = A_L - A_R$ (the differential absorbance), are induced by the field. H is measured in Tesla (T, 1 T = 10000 Gauss); b is the concentration in mol l^{-1} and l the pathlength in cm. Another unit common in the literature is the molar ellipticity (per unit field), $[\theta]_M$, which is related to $\Delta\epsilon_M$ as follows (for a unit field of 1 T): $[\theta]_M$ (deg cm^2 dmol^{-1} T^{-1}) = 100 θ/bl = 3300 $\Delta\epsilon_M$, where θ is the field-induced ellipticity (deg). When possible, we have provided sufficient information in the figure legends to allow the reader to convert from the reported units to $\Delta\epsilon_M$. A detailed discussion of units and a very useful table of conversion factors can be found in ref. 9.

C. COPPER

Compared to the amount of work devoted to the study of non-heme iron and cobalt containing bioinorganic systems (vide infra), relatively little MCD spectroscopy has been done on copper, despite the enormous interest in copper proteins. Since Cu(II) is d^9 and subject to a Jahn–Teller distortion in cubic symmetries, the ground state of a Cu(II) complex will always be an orbitally non-degenerate Kramers doublet. The MCD spectrum in the ligand field region should then be dominated by B and C terms. Most Cu(II) sites in proteins are low in symmetry, so again we expect that B and C terms should dominate. With few exceptions, the MCD spectra obtained on copper proteins were recorded at ambient temperature, therefore separating B_0 and C_0/kT contributions has not been possible. An additional unfortunate consequence is that the Cu(II) d–d transitions have generally not been resolved.

(i) Simple complexes

Kato first considered the MCD expected for vibronically allowed d–d transitions in tetragonal Cu(II) complexes [24]. He calculated the vibronically-allowed electric-dipole transition moments within the RS approximation and used the results to analyze the MCD spectra of $Cu(NH_3)_4^{2+}$, $Cu(en)_2^{2+}$ and $Cu(gly)_2^{2+}$ at room temperature. Experimental absorption and MCD spectra for $Cu(NH_3)_4^{2+}$ are shown in Fig. 3. Spectra of $Cu(en)_2^{2+}$ were very similar. The observed bands are almost entirely derived from B and C terms, with the B term dominant. Since the ground state is orbitally non-degenerate (but is spin degenerate) in tetragonal Cu(II) complexes, C_0/kT would be zero in the limit of zero spin–orbit coupling. Spin–orbit splitting of the ^2E_g excited state will produce non-zero C terms for the

$^2B_{1g} \rightarrow {}^2E_g$ transition (as mentioned in Section B). *C* terms can also occur via second-order spin–orbit coupling of an orbitally degenerate excited state to the ground state in these compounds. For the $^2B_{1g} \rightarrow {}^2E_g$ transition, Kato's calculation indicates that the *B* and *C* terms are approximately the same magnitude at room temperature. Because the $^2B_{1g} \rightarrow {}^2E_g$ transition is not resolved from $^2B_{1g} \rightarrow {}^2A_{1g}$ and $^2B_{1g} \rightarrow {}^2B_{2g}$, where no *C* terms are possible, the total dispersion comes mainly from *B* terms. In the $Cu(gly)_2^{2+}$ MCD spectrum, only a single negative band is observed of about the same intensity, despite the lower symmetry. MCD spectra for other Cu(II)–amino acid/peptide complexes have also been reported [25].

An instructive example of the use of MCD to determine the electronic structures of Cu(II) complexes is the study by Rival and Briat on CuX_4^{2-} (X = Cl, Br) [26]. Based upon examination of the room temperature spectrum and neglect of spin–orbit coupling, the two principal lowest energy bands were assigned to *A* terms arising from $^2T_1$ and $^2T_2$ states (in T_d symmetry). Subsequently low temperature data and a more complete theoret-

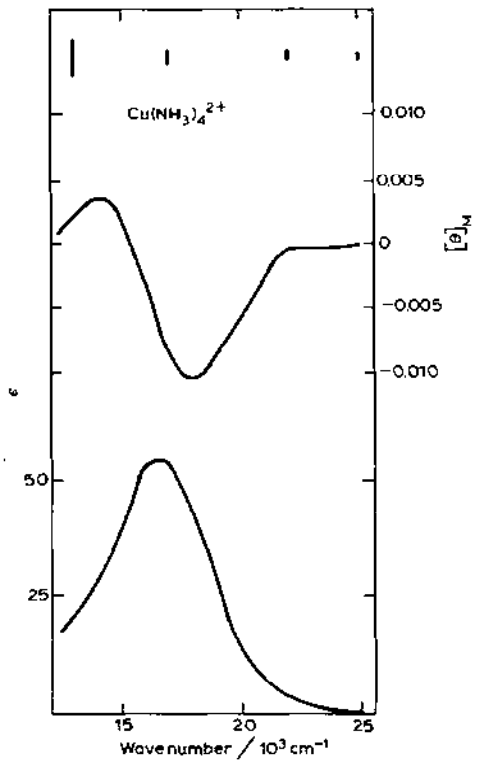

Fig. 3. The experimental MCD and absorption spectra of $Cu(NH_3)_4^{2+}$ in solution at room temperature. From ref. 24.

ical analysis based on the rigorous D_{2d} symmetry indicated that the bands actually were pseudo *A* terms composed of overlapping, oppositely-signed *C* terms. Analysis of the MCD signs and intensities together with polarized single-crystal absorption and reflection data [27] permitted detailed assignments of both *d–d* and charge transfer transitions [26,27]. Taken together, these papers illustrate what can be learned from MCD spectra at room temperature and at low temperature, and provide an excellent example of how MCD and polarized absorption spectroscopy complement each other.

(ii) Superoxide dismutase

Bovine erythrocyte superoxide dismutase was the first copper protein studied by MCD spectroscopy [28]. A broad negative band between 500–700 nm was observed, with minima at 595 and 640 nm. Negative activity was also apparent from ca. 450–330 nm. $\Delta\epsilon_M$ between 500 and 700 nm was significantly greater than $\Delta\epsilon_M$ of most Cu(II) complexes examined. More recently Rotilio et al. have reported MCD spectra of the native Cu–Zn enzyme and a derivative where Co(II) has been substituted for Zn(II) [29]. Overall their MCD spectrum is similar to that obtained earlier but some differences are noticeable. In particular, Rotilio et al. did not resolve two separate negative peaks between 500–700 nm; only a single negative minimum was observed. In addition, they report another negative band at 450 nm and a positive peak at 720 nm, but no activity at wavelengths less than ca. 400 nm. Thus MCD experiments have resolved at least two, and perhaps three, of the three (or four, in lower symmetry) expected *d–d* transitions of a tetragonal $Cu(II)N_4$ chromophore. These transitions are partly resolved in the absorption spectrum. Variable temperature experiments should be quite informative, particularly since the structure is known and the data can be used to interpret MCD data on other copper proteins.

(iii) Hemocyanin

Some studies have also been done on hemocyanin [30,31]. The first report covered only the UV and near-UV regions [30]. Even at a 7 Tesla field, practically no MCD could be detected at ca. 350 nm in oxyhemocyanin, where an intense absorption band ($\epsilon \sim 20000\ M^{-1}\ cm^{-1}$) associated with the binuclear copper–oxygen chromophore occurs. Absorption, CD and MCD spectra in the visible region of *Sepioteuthis lessoniana* hemocyanin at 293, 198 and 77 K have been recorded [31]. Only a weak, broad negative band between 500 and 700 nm was observed in the MCD spectrum. Although the band was weakly temperature dependent, the changes were proportional to those in the absorption spectrum, which apparently rules out

the involvement of *C* terms. Consequently, *B* terms are expected to dominate, since the symmetry is likely to be quite low. One conclusion of this work, that the Cu(II) ions in the binuclear active site are inequivalent, is probably incorrect as it was based on the misassignment of all five visible bands to Cu(II) *d–d* transitions. Some of these bands have more recently been assigned as charge-transfer transitions [32].

The oxygenated protein contains binuclear Cu(II) ions, but no EPR signal is evident indicating that the Cu(II) ions are antiferromagnetically coupled. Magnetic susceptibility experiments established that the ground state is diamagnetic and that the coupling is fairly large [33,34]. Therefore, no MCD saturation should be observable; such experiments would provide a useful check on the magnetic susceptibility results.

(iv) Blue copper proteins

Gray and co-workers have systematically examined the MCD spectra of several blue copper proteins in the visible and near-IR regions [35–40]. A typical spectrum in the visible region is shown in Fig. 4. Compared to the data for hemocyanin and superoxide dismutase, the principal band in Fig. 4 is approximately three times as intense. This is consistent with its assignment as an electric-dipole allowed ligand-to-metal charge transfer transition. *B* and *C* terms are probably responsible for the observed bands. Visible MCD spectra of plastocyanin, azurin, *Rhus vernicifera* laccase, ascorbate oxidase and ceruloplasmin are similar, on a per-copper basis [36–40]. Significant

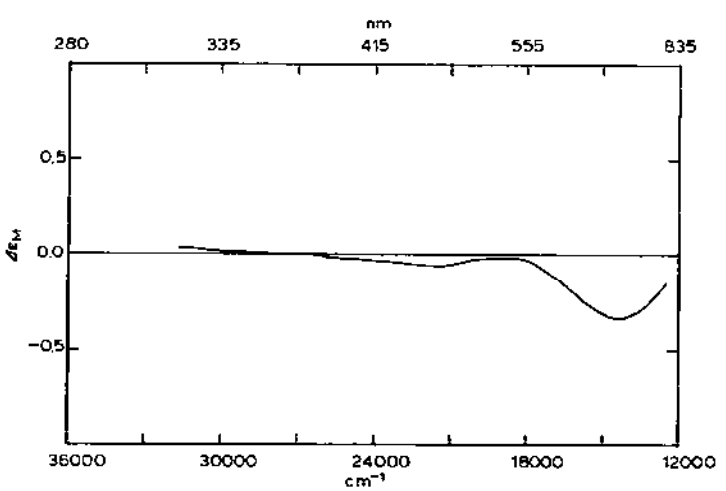

Fig. 4. MCD spectrum of *Rhus vernicifera* laccase in $\mu = 0.1$ M potassium phosphate buffer (pH 6.0) at room temperature. From ref. 36.

differences are apparent in the MCD spectra of stellacyanin (Fig. 5) and fungal laccase. These differences are intriguing because stellacyanin and fungal laccase may both contain Type 1 (blue) copper sites which are structurally different from the prototypical sites in azurin and plastocyanin. For instance, methionine has been demonstrated to be a Cu(II) ligand in plastocyanin and azurin [41,42], yet stellacyanin contains no methionine [43]. Fungal laccase has several spectral differences compared to all the other blue copper proteins, and by far the highest redox potential [36].

Near-IR MCD experiments detected Cu(II) *d–d* transitions in plastocyanin, stellacyanin and azurin that were weak in absorption and CD. These bands were less intense than the visible region MCD bands but were still more intense than the Cu(II) *d–d* bands of superoxide dismutase or hemocyanin, consistent with a more tetrahedral symmetry for the blue copper site. Unfortunately, no near-IR MCD beyond ca. 900 nm could be detected for the laccases at concentrations used for the CD measurements.

MCD spectra of ceruloplasmin complexes with N_3^- and SCN^- were also obtained (Fig. 6) [38]. Although anions bind to the Type 2 (non-blue) copper in ceruloplasmin, other experiments indicate that the blue sites are perturbed by binding. Clearly the MCD data are consistent with this idea as the negative band at ca. 14000 cm^{-1}, attributable to blue copper transitions in the native protein is evident but greatly reduced in magnitude. At present none of the transitions can be unambiguously assigned to specific copper centers. Recall that for a center with a Kramers-doublet ground state MCD saturation experiments yield the ground state g value. Since Types 1 and 2 copper are known to have different g values, this suggests immediately that saturation experiments might be used to assign the bands in Fig. 6 to specific copper sites by comparison of the MCD g values to those derived from EPR measurements. Further MCD studies of native and anion-bound ceruloplasmin should be very helpful in resolving the yet unsettled questions regarding some spectroscopic assignments and the nature and extent of the

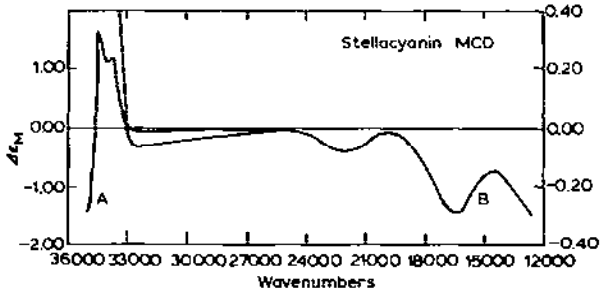

Fig. 5. MCD spectrum of *Rhus vernicifera* stellacyanin in deuterated phosphate buffer (pH 6.0) at room temperature. From ref. 38.

inequivalency between the two blue copper sites. Hervé et al. [44] propose that anion binding affects only one Type 1 site, whereas Dawson et al. [37] interpret their near-IR CD data obtained on the azidebound derivative as indicating that both Type 1 sites are perturbed. The fact that the visible MCD spectrum of ceruloplasmin is about twice as intense but no broader than the band in single blue copper proteins suggests that the electronic features responsible for the band are not grossly different in the two blue sites.

(v) Cytochrome c *oxidase*

MCD spectroscopy has proved extremely useful in characterizing the heme groups in cytochrome *c* oxidase. Recently MCD studies have provided new information about the copper centers [45,46], which we will now consider. Two important questions concerning the electronic state(s) of copper in cytochrome *c* oxidase have been addressed: (1) Is a Type 1 copper present? (2) Are heme a_3 and Cu_{a3} magnetically coupled in any way? Elegant work by Thomson and co-workers [45,46] has convincingly answered

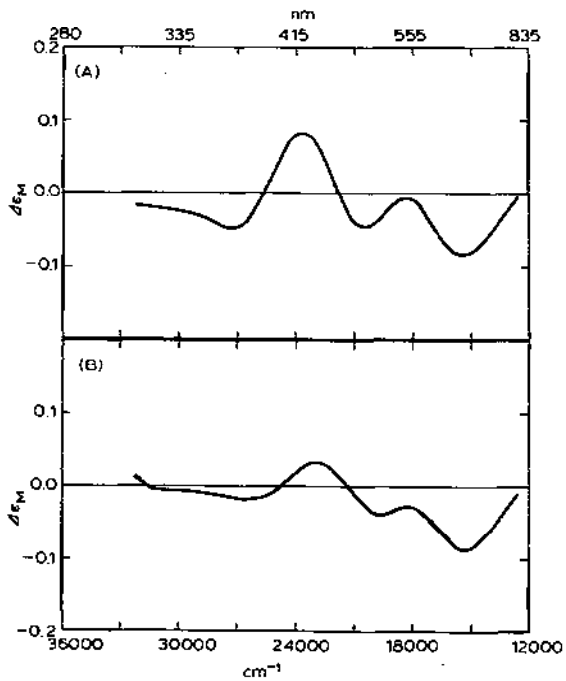

Fig. 6. (A) MCD spectrum of the ceruloplasmin–azide complex in 0.2 M sodium acetate (pH 5.5). (B) MCD spectrum of the ceruloplasmin-thiocyanate complex under the same conditions. From ref. 37.

the second question for the oxidized CN^- derivative, and provided essential data relevant to answering the first question.

Near-infrared CD and MCD experiments on the oxidized enzyme (Fig. 7) and other derivatives, together with titration data, are consistent with an assignment of the 840 nm band to a Cu(II) center [45]. Although high-spin heme a_3^{3+} will display transitions in this region in the oxidized enzyme, no evidence for heme transitions between 700–1300 nm was found in the oxidized CN^- derivative, when the 840 nm band was still prominent. This and other evidence suggests that the major contributor to the moderately intense negative band at 840 nm in Fig. 7 is Cu(II) [45]. However, the relative magnitudes of the CD and MCD bands of cytochrome oxidase in this region are very different from typical blue copper centers. In fact, the oxidase MCD is roughly 5–10 times that of blue copper signals but the CD of cytochrome oxidase is about 35–40 times less intense. It is likely that, if a blue copper ion is present in cytochrome *c* oxidase, significant structural differences exist compared to other blue copper proteins.

Saturation curves for the heme a_3 Soret MCD signal have also been obtained by Thomson et al. [46]. The results are briefly considered here because of their importance to the a_3/Cu_{a3} site structure in cytochrome *c*

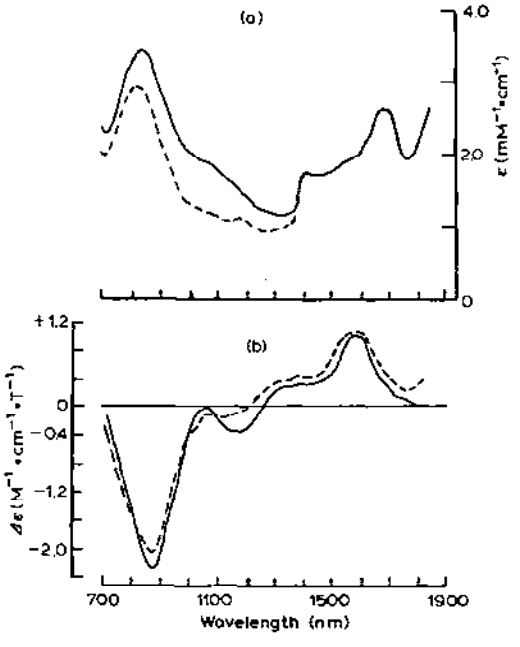

Fig. 7. Absorption (a) and MCD (b) spectra of oxidized cytochrome *c* oxidase derivatives at room temperature. (———) Oxidized enzyme; (- - - - - -) cyanide derivative. From ref. 45.

oxidase. Typical curves are displayed in Fig. 8. By subtracting these two curves Thomson et al. were able to generate the saturation curve for the heme a_3-CN^- form. Merely the observation of saturation conclusively rules out a diamagnetic $S = 0$ ground state for the heme a_3-CN/Cu_{a3} site. If the ground state was diamagnetic only the $S = 0$ state would be populated at 1.5 K (the lowest temperature used) so the MCD signal would vary linearly with the applied magnetic field. The data are completely consistent with an $S = 1$ ground state with an axial zero-field splitting (any rhombic field is probably less than 1 cm^{-1}) that results in a $M_S = \pm 1$ doublet at lower energy, with $M_S = 0$ at least 10 cm^{-1} higher in energy. On the other hand, Tweedle et al. analyzed their magnetic susceptibility data betwen 7–200 K in terms of a diamagnetic ground state that resulted from antiferromagnetic coupling between low-spin heme a_3 and $Cu(II)_{a3}$ [47]. At the present time the two results have not been reconciled. Further, Thomson and co-workers could find no way to reconcile antiferromagnetic coupling and a low symmetry with the experimental ground state [46]. They concluded that either Cu_{a3} ($S = 1/2$) and a_3-CN^- ($S = 1/2$) were ferromagnetically coupled to give $S = 1$ or that the Fe in a_3 is present as Fe(IV) $S = 1$ and Cu_{a3} is Cu(I). As

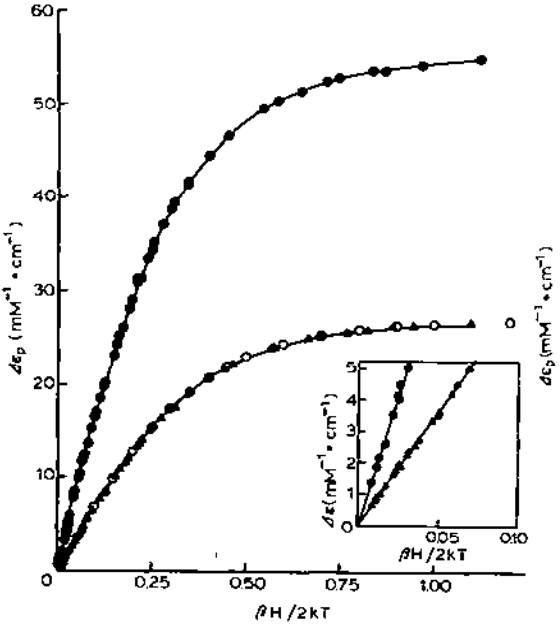

Fig. 8. MCD magnetization curves (i.e., plots of peak to trough intensity for the Soret-band MCD, $\Delta\epsilon_p$, versus $\beta H/2kT$) for the oxidized resting (▲) and oxidized cyanide (●) derivatives of cytochrome *c* oxidase. The insert shows an expresion of the region at low $\beta H/2kT$ values. From ref. 46.

data on Fe(IV) systems is very sparse, no choice between these two alternatives was made.

D. RARE-EARTH IONS

The discovery that lanthanides, particularly the trivalent ions, could substitute for Ca^{2+} in many different proteins has stimulated interest in the spectroscopic properties of these ions [48,49]. To date, effort has concentrated quite successfully on their use as luminescent probes. Given the extremely diverse and numerous roles of Ca^{2+} in biology, the opportunities in this field are enormous.

MCD measurements on lanthanide ions were first made several years ago. It was recognized early that the MCD dispersion could be straightforwardly related to the lanthanide-ion site symmetry. For example, the structure of aqueous Eu^{3+} could be determined by explicitly including crystal field effects in the analysis of the MCD transitions [50,51]. In this case the signs of particular A and C terms were consistent only with a D_{3h} structure. Moreover the absorption process, i.e. magnetic dipole versus electric dipole, could also be deduced. Görller-Walrand et al. have also recently surveyed the MCD spectra of several trivalent rare earth aqueous ions, with a view towards analytical applications [52]. Nd^{3+} displayed the largest $\Delta\epsilon_M$, as noted by others, although Dy^{3+}, Ho^{3+}, Eu^{3+} and Pr^{3+} all showed bands with $\Delta\epsilon_M > 1.4\ M^{-1}\ cm^{-1}\ T^{-1}$ in the visible region (and thus free of any protein MCD interference).

(i) Neodymium

Solution MCD spectra of several Nd^{3+} complexes have been measured in order to assess the utility of such measurements in elucidating metal-ion site structure [53]. The band shapes, signs and intensities were found to vary across the spectra; this suggests that the systematic study of MCD spectra versus coordination number, geometry and ligand identity would be useful in developing rare earth MCD spectroscopy as a Ca^{2+} active site probe. Generally bands in the Nd^{3+}-complex spectra were broader and less intense than the aquo ion spectra. No spectral features characteristic of coordination number or geometry from this limited set of spectra were evident, but clearly much more work is necessary before any final evaluation is made.

Donato and Martin reported the first application of Nd^{3+} MCD as a Ca^{2+} active site probe [54]. They examined Nd^{3+}-substituted parvalbumin and observed "...a uniquely different MCD of weak intensity", but, unfortunately, no spectra were shown. Donato and Martin [54] further suggested that the weak intensity might imply a high symmetry site. Other data do not

particularly support this suggestion. The MCD spectrum of Nd^{3+} bound to thermolysin has been measured by Holmquist and Horrocks [55] (Fig. 9). Nd^{3+} binding is known to occur via substitution at the Ca^{2+} binding sites. Only one Nd^{3+} was bound to thermolysin under the conditions employed. It is evident from Fig. 9 that the aqueous Nd^{3+} $^4I_{9/2} \rightarrow {}^4F_{7/2}$, $^4S_{3/2}$ transitions, near 740 nm, and the $^4I_{9/2} \rightarrow {}^2H_{9/2}$ transition at 794 nm are significantly affected upon complexation to thermolysin. Particularly interesting is the splitting of the prominent *A* term at long wavelength into three extrema.

(ii) Europium

Eu^{2+} substitution for Ca^{2+} at the S2 site in concanavalin A has been demonstrated by Homer and Mortimer [56]. Several features of their study indicate that Eu^{2+} MCD may prove highly successful as a method to probe Ca^{2+} sites. Most importantly, bands attributable to $f \rightarrow d$ transitions, from the $4f^7$–^8S ground state to excited states arising from the $4f^65d^1$ configuration, can be studied. These transitions are much more intense than *f*–*f*

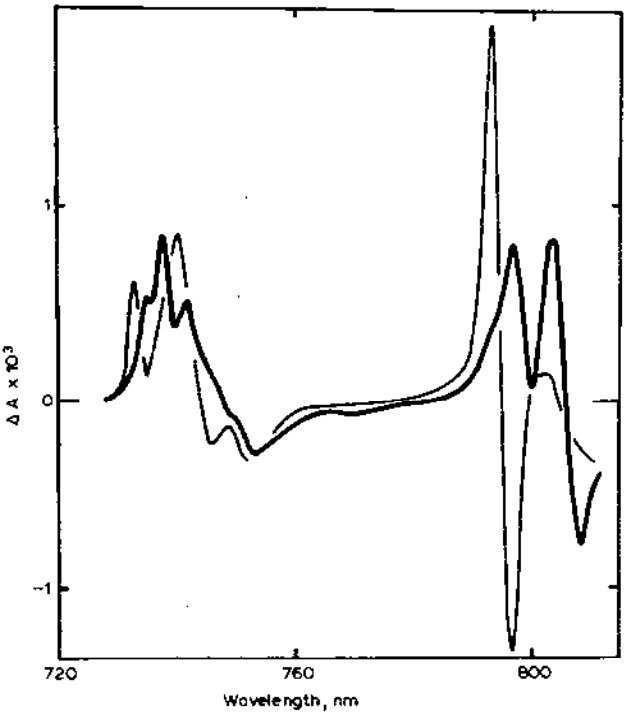

Fig. 9. Qualitative comparison of the MCD of aqueous Nd^{3+} (light line) and thermolysin-bound Nd^{3+} (heavy line). From ref. 97.

transitions in MCD spectra. In addition, $f \rightarrow d$ transitions are much more sensitive to changes in the ligand field, and hence changes in coordination number and geometry, than are $f \rightarrow f$ transitions. The MCD spectrum of concanavalin A in the presence of Eu^{2+} is shown in Fig. 10. The positive MCD feature near 370 nm has been assigned to aquo Eu^{2+} while the positive MCD band at 413 nm arises from Eu^{2+} bound to the protein. The time dependence apparently corresponds to a protein conformational change induced by Eu^{2+} binding that has also been observed by other techniques. The sensitivity of the MCD spectra of Eu^{2+} ions to structural changes in the metal site is well illustrated by these spectra. Additional features present in the MCD spectrum of Eu^{2+}–concanavalin A compared to the spectrum of aqueous Eu^{2+} may reflect a symmetry reduction in the S2 site, which is known to be seven-coordinate. The principal drawback in the use of Eu^{2+}

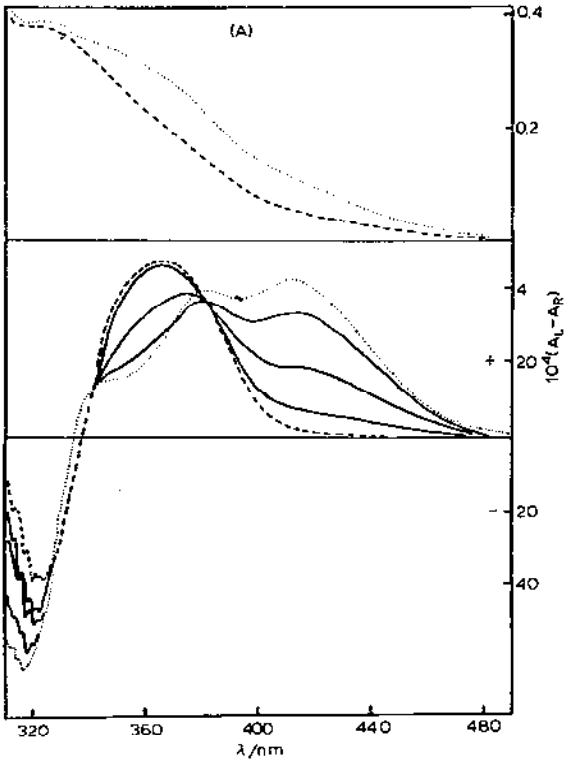

Fig. 10. Absorption (upper curves) and MCD (at 5.1 T) spectra of Eu^{2+} in the presence of concanavalin A at pH 5.5. (------), Apo-concanavalin A (5.7×10^{-4} M) with a ten-fold excess of Ca^{2+} and Mn^{2+} in a 0.5 cm cell 5 h after mixing (clearly Eu^{2+} does not bind to concanavalin A in the presence of Ca^{2+}). (———), Apo-concanavalin A (6.9×10^{-4} M) with Mn^{2+} (5.6×10^{-3} M) and Eu^{2+} (1.87×10^{-3} M) in the absence of Ca^{2+} in a 1.0 cm cell, 0.25, 1.25 and 3.25 h after mixing. (· · · · · ·), same conditions as (———), after 6 h. From ref. 56.

MCD is that Eu^{2+} is a powerful reductant that may be reactive with some proteins and can be oxidized by O_2, thus requiring anaerobic conditions.

(iii) Praseodymium

Pr^{3+} has also been employed to probe metal sites in concanavalin A. Most bands in the MCD spectrum of aqueous Pr^{3+} are red-shifted by 0.5–1.0 nm and decreased by approximately 20% in the presence of equimolar concanavalin A [57], in contrast to the much larger changes observed in the MCD spectra of Eu^{2+} or Nd^{3+} when bound to proteins. This is consistent with the suggestion that Pr^{3+} does not bind to the Ca^{2+} site, but to another site, S3, that consists of only two protein-derived ligands and hence may allow bound Pr^{3+} to maintain the high coordination number characteristic of the aqueous ion.

Despite these reports and the optimism of some investigators, the applications of rare earth ion MCD in bioinorganic chemistry do not appear to be increasing greatly; we are aware of no new reports appearing after these studies.

E. COBALT AND OTHER METAL IONS

Unquestionably the application of MCD spectroscopy to Co(II)-containing metalloproteins has been extraordinarily successful, particularly in the determination of metal-site geometry and coordination number. Owing to the fact that Co(II) may be substituted for Zn(II), which has very limited chromophoric properties, MCD has been very widely applied to such systems. Co(II) has also been substituted for Cu(II), Fe(II), Mg(II), Mn(II) and Ca(II), thus extending its use as a probe and permitting informative comparisons between metal sites containing Co(II) and other transition metal ions. Much of the credit for the development of this area belongs to Vallee, Holmquist and co-workers who recognized early on the potential of MCD spectroscopy and have systematically applied it to the study of a large number of Co(II)-containing proteins. This work has been reviewed previously [9–12]; here we will concentrate on work reported since the most recent review and on aspects heretofore only briefly considered.

(i) Model systems

Applications of MCD to Co(II)-containing biochemical systems have relied heavily on studies of simple Co(II) complexes. The MCD of tetrahedral CoX_4^{2-} (X = Cl, Br, I) [26,27,58,59] and octahedral $Co(H_2O)_6^{2+}$ [60,61] have been examined in some detail. Both the $^4A_2 \rightarrow {}^4T_1(P)$ transition

in CoX_4^{2-} and the $^4T_{1g} \rightarrow {}^4T_{2g}$ transition in $Co(H_2O)_6^{2+}$ (the principal d–d transitions in the visible range) display MCD spectra dominated by C terms. In the former case, spin–orbit splitting of the excited state largely determines the C term magnitude, while in the latter case spin–orbit coupling in the ground state is most important. Katô and Akimoto examined several tetrahedral Co(II) complexes, concluding that the major contribution to the MCD arises from C terms and, importantly, that spin–orbit coupling has a larger effect upon the MCD than do low symmetry components in the effective ligand field [62]. In addition, the MCD of many other octahedral, tetrahedral and five-coordinate Co(II) complexes have been systematically examined [63]. The spectra were characteristic for each coordination geometry and were insensitive to small geometrical distortions. This may be a consequence of the greater contribution of spin–orbit coupling, compared to low symmetry effects, in determining the overall MCD dispersion in Co(II) complexes. It is difficult to overestimate the importance of these results for investigations of Co(II)-containing metalloproteins, as it is possible to deduce metal-site structure by comparing Co(II) protein MCD spectra with spectra from simple Co(II) complexes. Deductions of site structure based on MCD have been consistent with the X-ray crystallographic results, when such structures have been available.

(ii) Cobalt-substituted zinc proteins

Co(II) metalloprotein MCD were first reported by Vallee and co-workers [64,65]; very shortly thereafter MCD spectra of Co(II) carbonic anhydrase were reported by Coleman and Coleman [66]. Subsequently, the number of protein metal sites probed by Co(II) MCD increased rapidly. In a majority of cases, a pseudotetrahedral geometry for the Co(II)-substituted zinc site was most consistent with the MCD data from models. Some examples are: carboxypeptidases [64,65,67–70], thermolysin [71], D-lactate dehydrogenase [72], bovine erthyrocyte superoxide dismutase [29] and liver alcohol dehydrogenase [73]. Six-coordinate "octahedral-like" sites were deduced for the structural (Zn(II)) and regulatory (Mg(II)) metal sites in *E. coli* alkaline phosphatase [74,75], the activating divalent metal site in rabbit muscle pyruvate kinase [76] and the Mn(II) site in concanavalin A [77]. Typical MCD spectra are shown in Figs. 11 and 12, for a pseudotetrahedral and octahedral site, respectively.

Not every case has been unambiguous, however. One of the first enzymes examined, Co(II) carbonic anhydrase, proved problematical. At low pH and in the presence of inhibitors (e.g. anions), the MCD spectrum was consistent with a pseudotetrahedral, four-coordinate geometry [65,66]. At alkaline pHs the spectrum was quite different (Fig. 13). Coleman and Coleman [66] first

interpreted this spectrum in terms of a trigonally distorted tetrahedral geometry, with the negative bands at 618 and 642 nm assigned to enhanced $^4A_1 \rightarrow {}^2T_1(G)$, $^2E(G)$ transitions, respectively. However, the observed MCD spectrum at pH > 7 (Fig. 13) is quite reminiscent of spectra displayed by five-coordinate Co(II) complexes. In fact, the question of four- versus

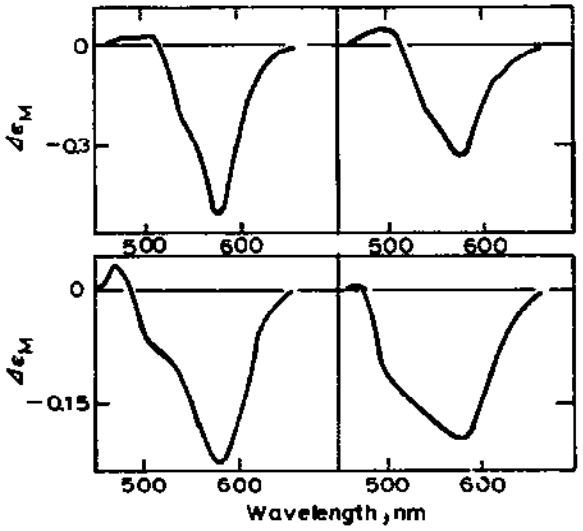

Fig. 11. MCD spectra of Co(II)-substituted zinc metalloenzymes containing "tetrahedral" Co(II). Upper left, carboxypeptidase A; upper right, carboxypeptidase P; lower left, thermolysin; lower right, *Bacillus cereus* neutral protease. From ref. 10.

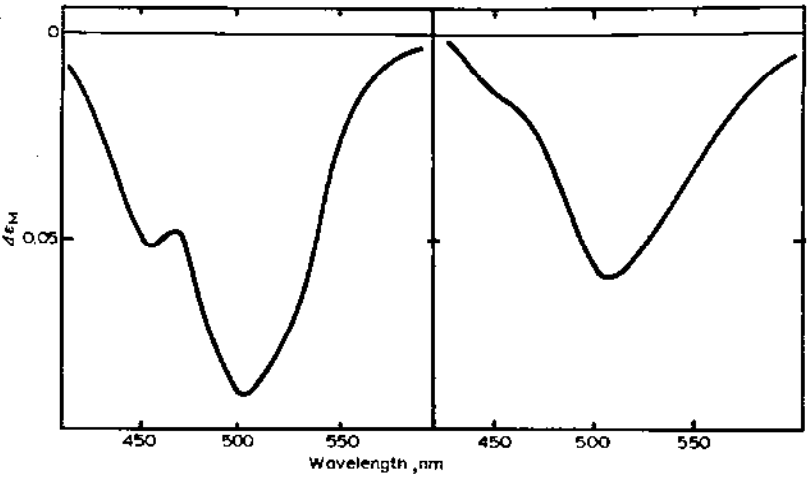

Fig. 12. MCD spectra of Co(II) substituted metalloproteins containing "octahedral" Co(II). Concanavalin A (left) and pyruvate kinase (right). From ref. 10.

five-coordination in carbonic anhydrase has been the subject of considerable debate (see ref. 78, for example). An X-ray structure, on the Zn(II) enzyme crystallized at pH 8, indicates a very distorted tetrahedral geometry, which is little affected by the addition of a sulfonamide inhibitor [79]. It is important to note that some of the pseudo-tetrahedral Co(II) complexes examined by Katô also have two negative bands in the MCD spectra, a result generally interpreted as indicative of five-coordination, so the present MCD data permit no definitive conclusion.

MCD spectra of Co(II)–Cu(II) bovine erythrocyte superoxide dismutase and the cyanide complex of Co(II) carbonic anhydrase are very similar [29,65]. Since the zinc (Co(II)) site in the superoxide dismutase is known to be approximately tetrahedral, this geometry would appear to be more likely for the carbonic anhydrase metal site as well. A thorough investigation of the temperature-dependence could be conclusive. Coleman and Coleman [66] observed that all the visible MCD bands in the MCD spectrum of Co(II) carbonic anhydrase (and its cyanide complex) at pH 9.0 were reciprocally temperature dependent over the range 274–314 K and were therefore assigned as *C* terms (Fig. 14). This is consistent with the theoretical and

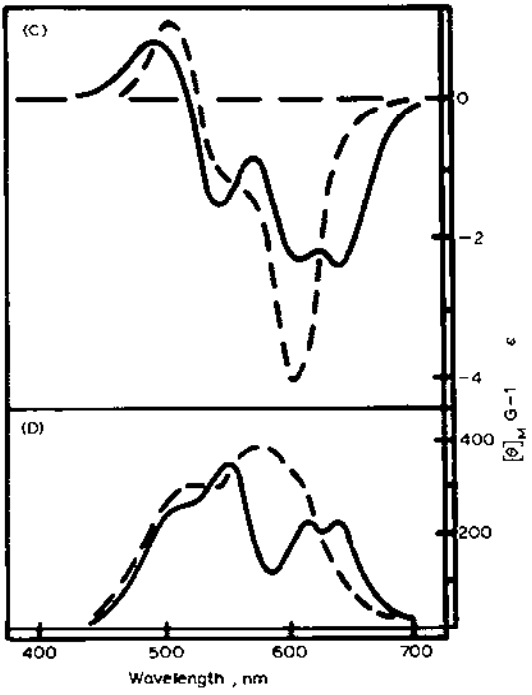

Fig. 13. Absorption (bottom) and MCD (top) spectra of Co(II) carbonic anhydrase at pH = 8 in the absence (———) and presence (- - - - -) of the inhibitor acetazolamide. From ref. 12.

experimental results on tetrahedral Co(II) complexes mentioned previously. In contrast, the lowest energy MCD band of the five-coordinate $Co(Et_4dien)Cl_2$ complex was not temperature dependent, indicating that it is principally a *B* term [63]. Thus variable temperature MCD experiments may distinguish very distorted tetrahedral geometries for Co(II) from five-coordinate structures. Clearly more five- and four-coordinate Co(II) complexes need to be examined (a detailed experimental and theoretical treatment of a five-coordinate complex would be especially helpful) and spectra obtained over a much larger temperature range, before any conclusion based on variable temperature MCD is justified.

Co(II) alkaline phosphatase from *E. coli* is another enzyme that displays somewhat ambiguous MCD spectra. Actually the protein has four Zn(II) sites and two Mg(II) sites [80]. Two of the metal sites give rise to Co(II) MCD spectra that are consistent with an "octahedral-like" geometry [74]; metal ions in these sites have a structual function. When Co(II) is substituted into the two catalytic Zn(II) sites a MCD spectrum results that is again consistent with a pseudotetrahedral or five-coordinate structure, and resembles that of Co(II) carbonic anhydrase (vide supra) [74,81]. Mg^{2+} ions have important regulatory effects. When no Mg^{2+} is present, the MCD spectra indicate that the structural sites are occupied in the 1-Co(II) and 2-Co(II) forms whereas in the presence of Mg^{2+}, the "five-coordinate-like" geometry predominates in these same forms [74]. Evidently Mg^{2+} influences metal ion

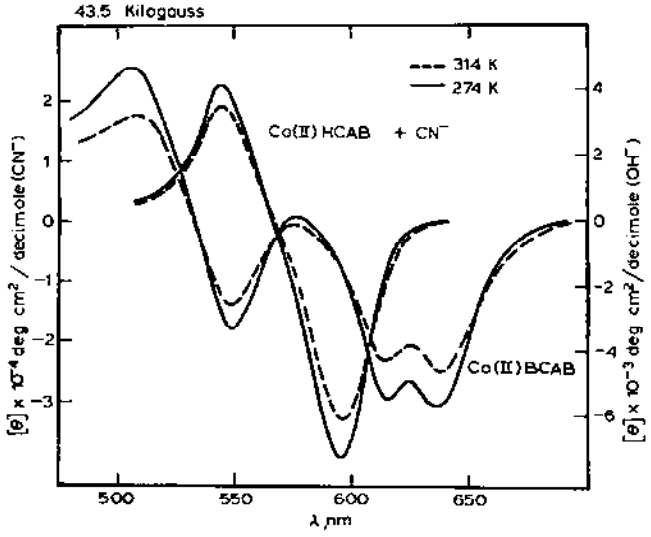

Fig. 14. MCD (at 4.35 T) of Co(II) bovine carbonic anhydrase B (BCAB) and Co(II) human carbonic anhydrase B·CN^- (HCAB+CN^-) as a function of temperature; (———) 274 K; (- - - - - -) 314 K. From ref. 66.

binding by alkaline phosphatase. Adding Mg^{2+} to the four-Co(II) enzyme merely increases $\Delta\epsilon_M$. Co(II) may also be substituted for Mg(II) and MCD indicates that the Mg(II) sites are octahedral, as expected [74]. Binding HPO_4^{2-} alters the MCD of the catalytic sites but not that of the structural sites. Interestingly, the changes in the MCD spectrum upon HPO_4^{2-} complexation are minor compared to changes in the CD spectrum indicating that changes in the latter spectrum reflect primarily differences in overall protein conformation around the metal site, rather than any substantive change in the metal-ion structure [81].

(iii) Cobalt-substituted copper proteins

Co(II) has also been substituted into copper sites in metalloproteins. Substitution of Co(II) for Cu(II) in bovine plasma amine oxidase has been reported [82]; the resulting MCD spectrum was consistent with a tetrahedral type geometry for Co(II). However, further work is needed to establish conclusively that the Co(II) binding site is a copper site, especially since Cu(II) has a tetragonal structure in native amine oxidases [83].

Co(II) substitution for copper in the binuclear copper site of squid and horseshoe crab hemocyanins has recently been reported [84,85]. Either 1 mol or 2.6 mol of Co(II) per mol active site was incorporated in squid hemocyanin, depending upon the procedure to remove excess Co(II) [84]. In the former case absorption and MCD spectra were consistent with a tetrahedral metal site, while in the latter case both tetrahedral and octahedral Co(II) sites were occupied. Two moles of Co(II) per mole of active site were incorporated into the four horseshoe crab hemocyanins [85]. All these Co(II) hemocyanins displayed MCD spectra typical of distorted tetrahedral geometries. Since no compelling evidence that Co(II) actually occupies the copper sites has been presented, the conclusion that the Co(II) geometries resemble those around Cu(I) in deoxyhemocyanin (oxyhemocyanin is known to contain tetragonal Cu(II) [32,86]) must be regarded as tentative.

An illustrative example of this substitution was the study of Co(II) substituted blue copper proteins by Gray and co-workers [87–89]. Visible and near-IR MCD were reported for Co(II) derivatives of azurin, plastocyanin and stellacyanin (Fig. 15) [89]. Comparison of the visible MCD to that of Co(II) model complexes indicated that a distorted tetrahedral metal site was present in all three proteins. Further, the pseudo A term present in the near-IR MCD spectra (Fig. 16) is completely consistent with distorted tetrahedral geometry, as spin–orbit coupling in the $^4A_2 \rightarrow {}^4T_1(^4F)$ transition of a tetrahedral d^7 ion will give C terms of opposite sign. Observation of the $^4A_2 \rightarrow {}^4T_1(^4F)$ transition in the near-IR permitted assignment of the visible bands to low symmetry split components of the $^4A_2 \rightarrow {}^4T_1(^4P)$ transition.

The MCD spectra for all three proteins were qualitatively very similar, indicating that the metal sites have similar structures in all three proteins, a result that has been confirmed by spectroscopic experiments and X-ray crystal structure determinations of plastocyanin and azurin. Again we note that the CD spectra are quite different for the three proteins both in the visible and near-IR regions.

(iv) Metal–sulfur chromophores

An additional important result of the work by Gray and co-workers [87–89] was the first observation of S → Co(II) LMCT transitions in the near-UV. Although evident in the absorption spectra, these transitions are much better resolved in the MCD spectra. At least two LMCT transitions were observed for each protein. In a distorted tetrahedral complex, four

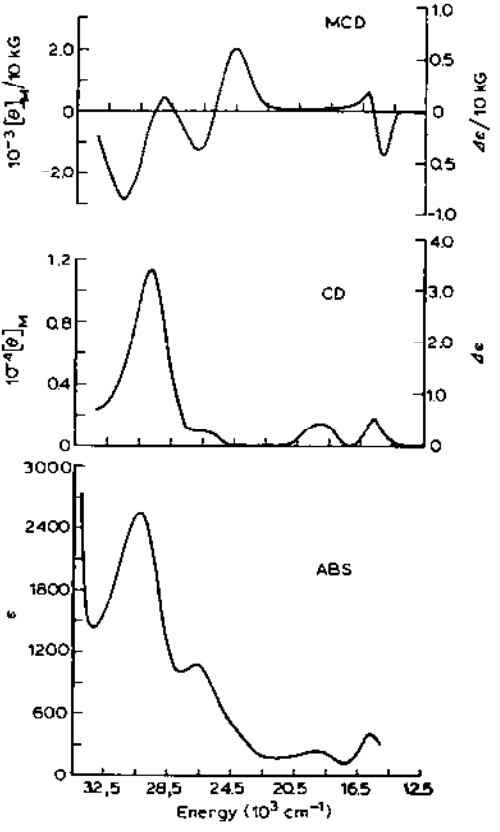

Fig. 15. Absorption, CD and MCD spectra of Co(II) azurin in the UV–visible region at room temperature and pH = 8. From ref. 89.

transitions [$S(\pi,\sigma) \rightarrow d_{xy}, d_{x^2-y^2}$] are possible. Analogous bands have been observed in the MCD spectra of Co(II)-substituted rubredoxin [90], alcohol dehydrogenase [72,73], β-lactamase II [91] and two metallothioneins (Fig. 17) [92,93]. The Co(II) metallothionein spectra indicate that the metals are in distorted tetrahedral sites with a larger distortion for the rabbit metallothionein. In the near-UV region, both are quite similar to the MCD spectrum of Co(II) rubedoxin, where it is known that four cysteine sulfurs are metal ligands in the native protein. In addition, the charge-transfer bands in the absorption spectra of the Co(II) metallothioneins were closely similar to those displayed by Co(II) tetrathiolate complexes. Thus four Co(II)–S bands are likely present in the metallothioneins as well [92].

Ni(II) metallothionein was also prepared [93]. Although absorption and CD spectroscopy failed to unambiguously resolve the Ni(II) d–d bands at 23°C, MCD spectroscopy at the same temperature clearly resolved a band at 710 nm assigned to a $^3T_1(F) \rightarrow {}^3T_1(P)$ ligand-field transition. A band at this energy was considered diagnostic of tetrahedral coordination around Ni(II). S → Ni(II) LMCT bands were also observed considerably red-shifted from

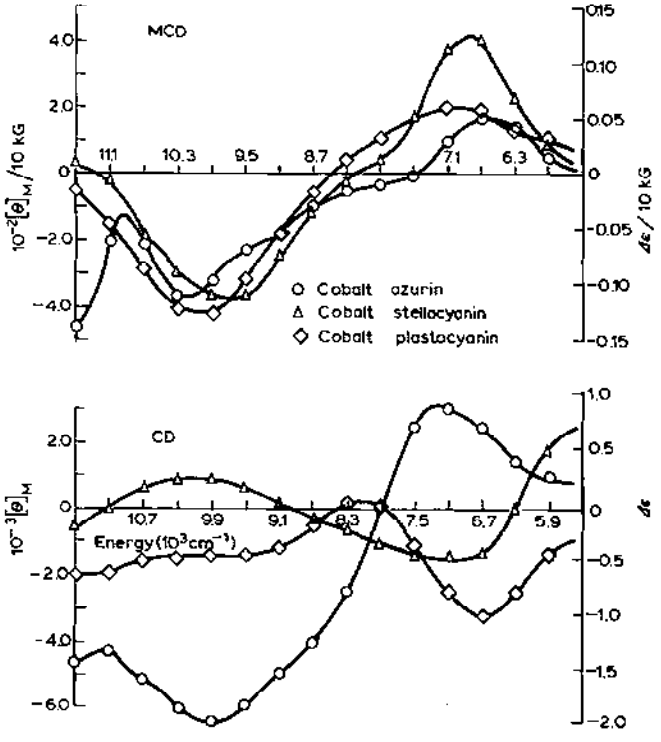

Fig. 16. CD and MCD spectra in the near-IR region for the Co(II) derivatives of stellacyanin (△), plastocyanin (◇) and azurin (○). From ref. 89.

the corresponding bands in the Co(II) metallothionein spectra. This is the first example of MCD obtained on nickel in a biological system. The richness and utility of the spectra should encourage the development of Ni(II) as a probe chromophore.

One thiol ligand to cobalt is suggested for β-lactamase II [91]. Its MCD spectrum in the visible region is remarkably similar to that of Co(II) carbonic anhydrase. Since the energy of LMCT transitions will also depend on geometry, the fact that the S → Co(II) energy in β-lactamase II is close to the energies for distorted tetrahedral sites suggests that the ambiguous visible MCD observed for both proteins is actually associated with a distorted tetrahedral site geometry.

Transitions associated with thiolate/disulfide-d^{10} metal chromophores in metallothioneins can be observed at higher energies (Fig. 18) [94,95]. This spectrum serves as a good example of the capability of MCD spectroscopy to resolve additional information from relatively featureless absorption spectra.

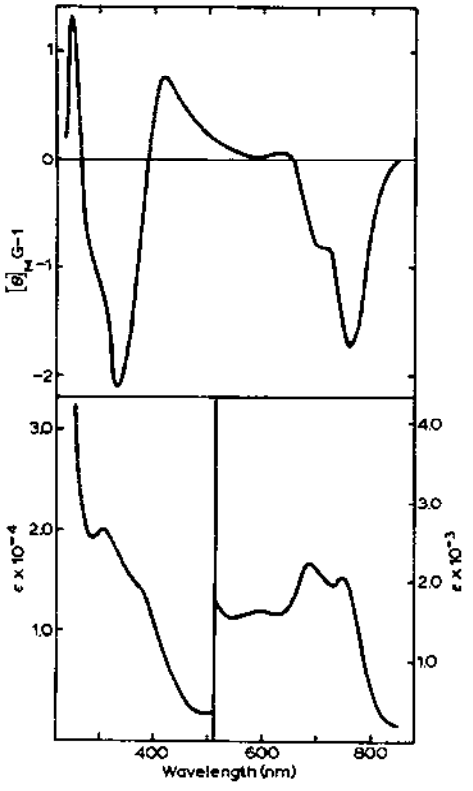

Fig. 17. MCD (top) and absorption spectra (bottom) of Co(II) metallothionein. Note that $[\theta]_M$ is based on the moles of protein; the stoichiometry is given as 6–7 mol Co(II)/mol protein. From ref. 92.

MCD has also been used to characterize the metal centers in bismuth induced metallothioneins that contained copper or zinc in addition to bismuth [96]. However, as is evident from a comparison of Figs. 17 and 18, considerably greater information is potentially available by substituting Co(II), or another metal ion with an unfilled *d*-shell for a d^{10} metal ion.

Holmquist and Vallee have elegantly exploited the distinctive MCD spectral features of the Co(II)–S chromophore to test metal-coordinating substrate analogs as inhibitors [97]. The spectra of Co(II) thermolysin in the presence of the thiol containing peptide 2-mercaptoacetyl-l-Phe-l-Ala (Fig. 19) clearly establish RS–Co(II) coordination indicating that this reagent is an active-site directed inhibitor. Further, the MCD is most consistent with a tetrahedral geometry, consistent with simple ligand substitution of a H_2O molecule on the metal ion. Similar results were obtained for other thiol containing substrate analogs and for carboxypeptidase. Such experiments provide a powerful method to test substrate ligation and to map metalloenzyme active sites. Vallee's laboratory also has recently reported the characterization by MCD, EPR and absorption spectroscopy of an intermediate

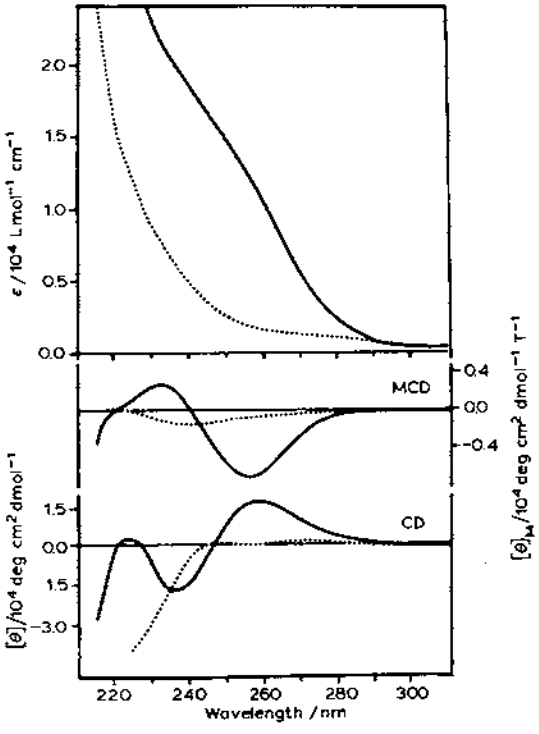

Fig. 18. Absorption (top), MCD and CD of Cd, Zn metallothionein at pH 8.5 (———) and pH 2.3 (· · · · · ·). $[\theta]_M$ is based on the protein concentration. From ref. 94.

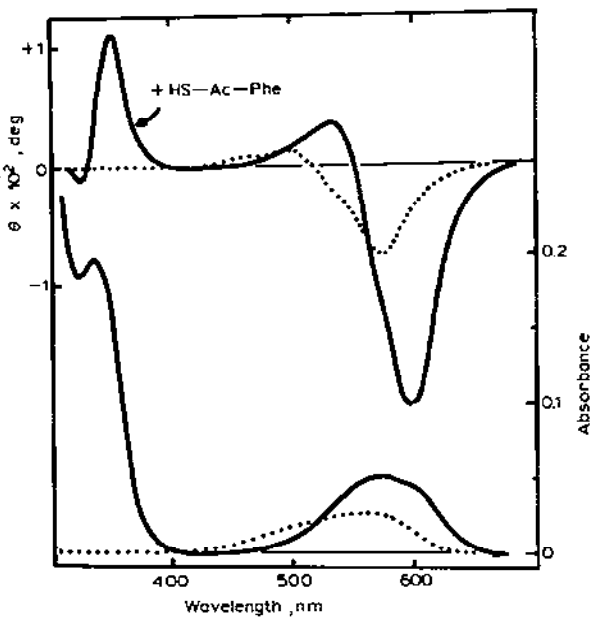

Fig. 19. Absorption (lower) and MCD spectra (at a magnetic field of 4 T) of Co(II) substituted carboxypeptidase A (2.8×10^{-4} M) in the absence (· · · · · ·) and presence (———) of the inhibitor 2-mercaptoacetyl-D-phenylalanine (HS–Ac–Phe). Adapted from ref. 97.

in the reaction of Co(II) carboxypeptidase with a model peptide [98]. Since many Co(II) enzymes display at least part of the native catalytic activity, MCD may prove extremely useful in cryoenzymology as a powerful means of investigating intermediates.

F. NON-HEME IRON

Non-heme iron proteins of the iron–sulfur type have been extensively studied and are structurally well characterized [99]. Proteins with iron centers having one, two and four irons tetrahedrally coordinated with zero, two and four inorganic sulfide ligands, respectively, and four cysteinate ligands are present in the electron transfer chains of most organisms. Recently, a three iron: three sulfur functional unit has been described [100]. Non-heme iron proteins that do not fall into these categories are also well known including the oxygen transfer protein hemerythrin, the iron transfer protein transferrin, numerous oxygenase enzymes and more. Most of these proteins can exist in at least two oxidation states. The study of these proteins with MCD spectroscopy can serve several purposes in addition to being of considerable use in the determination of the electronic structure of the iron

centers. In particular, by examining structurally characterized iron–sulfur proteins, it is possible to establish diagnostic spectral features to be used to ascertain the structures of iron centers in iron–sulfur proteins of unknown composition. Further, the use of MCD spectroscopy can help delineate reasonable structural possibilities for uncharacterized iron centers such as in non-heme iron oxygenase enzymes by comparison of the spectral properties of the proteins with those of structurally characterized model systems.

The first examination of the magnetic optical activity of a non-heme iron protein was by Marlborough et al. [101] who studied the magnetic optical rotatory dispersion (MORD) of spinach ferredoxin, a Fe_2S_2 protein. Although the techniques of MORD and MCD are closely related, all subsequent studies of the magnetic optical activity of non-heme iron proteins have been with MCD spectroscopy. Consequently, the study of Marlborough et al. will not be discussed further.

(i) One-iron iron–sulfur proteins and model systems

As part of a survey of the MCD properties of non-heme iron proteins Ulmer et al. reported the room temperature MCD spectra (300–700 nm) of oxidized and reduced rubredoxin from *Clostridium pasteurianum* in 1973 (Fig. 20A) [102]. Eaton and Lovenberg [103] published essentially the same spectra (obtained by Dr. David Ulmer) in the same year in a review article on rubredoxin. In 1977, Rivoal et al. [104] examined oxidized rubredoxin at room temperature and obtained a very similar spectrum to that reported by Ulmer et al. [102]; in addition, they examined oxidized rubredoxin at low temperature (6.1–17.2 K). Very recently, Johnson et al. [105] have examined oxidized and reduced rubredoxin and desulforedoxin from *Desulfovibrio gigas* by MCD spectroscopy at variable temperature down to 16 K. No further work has appeared on rubredoxin to date. Hatano and co-workers [106,107] have reported the MCD spectra of four iron complexes that may be models of the ferric site in rubredoxin.

The MCD spectra of rubredoxin (Fig. 20A) are quite distinctive. For reduced *Clostridium* protein, a peak is observed at 335 nm and a trough at 308 nm; no MCD has been observed above ca. 375 nm. These positions correspond well to absorption maxima seen at 312 and 335 nm [103] suggesting that the MCD features observed are due to two *B* or, more likely, *C* terms of opposite sign rather than a negative *A* term centered at 326 nm. The presence of *C* terms has been confirmed by Johnson et al. [105] who recently measured the MCD spectra of reduced rubredoxin and desulforedoxin (another one iron iron-sulfur protein), both from *Desulfovibrio gigas*, as a function of temperature down to 17.5 K. Both spectra are temperature dependent (the intensities of the major features increase by a

factor of 4–5) and are generally similar in shape and band position to the room temperature spectrum of the reduced *Clostridial* protein (Fig. 20) although somewhat different from each other in detail. The authors attributed the differences to variations in the low symmetry distortions of otherwise similar coordination structures [105]. A similar suggestion had previously been made to explain the differences in the Mössbauer spectra and zero-field splitting parameters of the two proteins [103].

The MCD spectrum of oxidized rubredoxin (Fig. 20A) is much more complicated. Positive peaks (or shoulders) are seen at approximately 308, 374, 519 and 587 nm. An additional shoulder at 609 nm is seen by Ulmer et al. [102], but not by the other two laboratories [103–105]. Troughs are seen

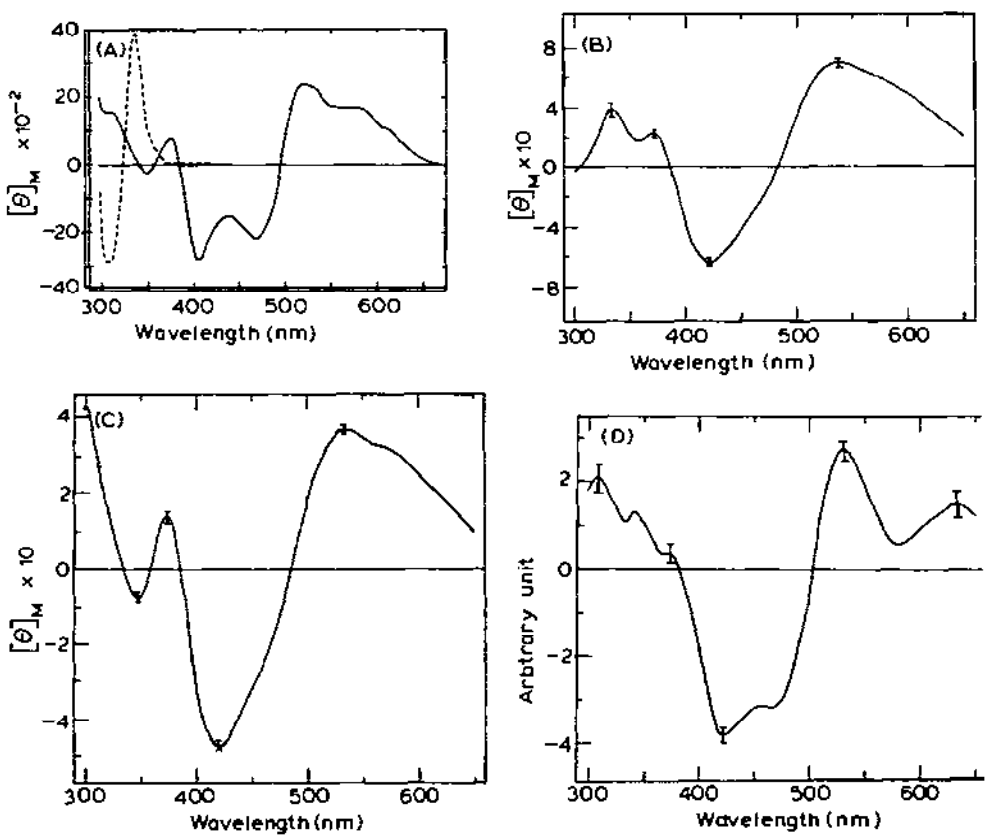

Fig. 20. (A) MCD spectra (normalized to 1 kilogauss) of oxidized (———) and reduced (- - - - - -) rubredoxin. From ref. 102. (B) MCD spectrum (normalized to 1 Gauss) of 1,4-butanedithiol–iron(III). Adapted from ref. 107. (C) MCD spectrum (normalized to 1 Gauss) of 1,6-hexanedithiol–iron(III). Adapted from ref. 107. (D) MCD spectrum of *o*-xylyl-α,α'-dithiol–iron(III). This data was obtained by mixing the ligand, sodium methoxide and ferric chloride (0.15 mM) in DMF in molar ratio of 10:10:1. Adapted from ref. 107.

at ca. 355, ca. 406 and ca. 467 nm. All of these features are temperature dependent [104] suggesting *C* term origins. The derivative shaped curves centered at ca. 383 and ca. 493 nm were assigned to oppositely-signed *A* terms [103,106,107]. No new transitions are seen at low temperature, merely intensification with concomitant sharpening of the spectral features. As in the case of reduced *Desulfovibrio gigas* rubredoxin and desulforedoxin, subtle distinctions are seen between the MCD spectra of their oxidized forms as a function of temperature down to 16 K [105]. Although both spectra are overall quite similar to that reported for oxidized *Clostridial* rubredoxin (Fig. 20A), the two positive peaks in the 500–600 nm region of the spectrum of oxidized desulforedoxin are not as well separated. Differences in the low symmetry distortions of the metal site were again cited as cause for these subtle distinctions [105].

As mentioned above, Hatano and co-workers have twice reported the MCD spectra of iron–sulfur model complexes for oxidized rubredoxin [106,107]. These complexes were prepared by addition of 1,2-ethanedithiol, 1,4-butanedithiol, 1,6-hexanedithiol and *o*-xylyl-α,α'-dithiol to ferric chloride. Despite the fact that all four species exhibit absorption spectra that are generally similar to that of rubredoxin [103], only the latter three (Figs. 20B–D) have MCD spectra that are at all close to that of the protein [102–106]. This is a good example of the increased "fingerprinting ability" of MCD relative to UV–visible absorption spectroscopy for establishing whether a metal complex is, in fact, a good model for a particular protein metal site. In this regard, the hexane and xylene dithiol ferric model complexes appear to be quite good, although not exact, models for ferric rubredoxin, while the match for the butanedithiol complex is not as good. As studies of the butanedithiol complex by EPR spectroscopy have shown it to have a rubredoxin-like core structure [108], it may be that MCD is superior to EPR spectroscopy in discriminating among possible model complexes for iron–sulfur sites in proteins. The intensities of the spectrum of the hexanedithiol complex more closely match those of the protein than does the butanedithiol adduct. Unfortunately, the intensities of the xylene dithiol complex were not determined.

Future efforts to use MCD spectroscopy to study rubredoxin can readily be foreseen. Both the oxidized and reduced proteins have weak, ligand field absorption bands in the near-IR [103,109] that should be examined and compared to the spectra of synthetic analogs [109]. In the case of the oxidized protein, in addition to characterization of the near-IR region, the weak transition at 745 nm [103] should be studied. Finally, no model compounds for reduced rubredoxin [109] have been investigated with MCD spectroscopy. Given the documented sensitivity of the technique to subtle changes in the iron chromophores, MCD studies would be useful in evaluat-

ing the integrity of such models. In addition, the recently prepared model for ferric rubredoxin [110] with four monoalkylthiol ligands, possibly the best ferric rubredoxin model to date, should be characterized by MCD for the reasons just outlined. Finally, rubredoxins from other sources (such as *Psuedomonas oleovorans*) should be examined in order to further test our understanding of the electronic properties of this class of iron–sulfur proteins.

(ii) Two-iron iron–sulfur proteins and model systems

Iron–sulfur proteins of the Fe_2S_2 classification and model compounds of that composition have been investigated by MCD spectroscopy in several laboratories. The proteins examined include two-iron ferredoxins from spinach [102,111,112] and from *Spirulina maxima* [102,114] as well as adrenodoxin [102,112], putidaredoxin [102,113] and xanthine oxidase [102,115]. The latter protein has recently been shown to contain Fe_2S_2 units by core extrusion [116,117]; molybdenum and flavin cofactors are also present. Spectra for the proteins were usually reported for both the oxidized and reduced states. In several cases, low temperatures have been used to better define the spectra and to look for MCD *C* terms which are expected for the paramagnetic reduced Fe_2S_2 state. Most of the spectra cover only the 300 to 650 nm range, a few go to 800 nm and the spectrum of oxidized putidaredoxin [113] extends to 1200 nm. Four model complexes possibly having structures similar to the oxidized proteins have also been examined at ambient temperature [107].

The MCD spectra of the oxidized Fe_2S_2 unit are generally similar regardless of source. To illustrate this point, the spectra of oxidized putidaredoxin and *Spirulina maxima* ferredoxin [112] are reproduced in Fig. 21. As can be seen, both contain four positive bands in the 400–800 nm region (ca. 425, ca. 485, ca. 530 and ca. 700 nm), two negative transitions between 340 and 400 nm (ca. 350 and ca. 380), and a positive feature at ca. 330 nm. For putidaredoxin, a negative trough is observed at ca. 300 nm, beyond the region examined for the ferredoxin. The overall intensities of the two spectra are quite similar and are approximately ten times less than those observed for rubredoxin (vide supra). Subtle distinctions are seen in that the spectrum

---

Fig. 21. (A) MCD spectra (normalized to 1 Tesla) of oxidized (- - - - - -) and reduced (———) putidaredoxin. Adapted from ref. 113. (B) MCD spectra (normalized to 1 Tesla) of oxidized (- - - - - -) and reduced (———) *Spirulina maxima* ferredoxin. Adapted from ref. 113. (C) MCD spectrum (normalized to 1 Gauss) of 1,4-butanedithiol–iron(III)–S*. This data was obtained by mixing the ligand, sodium sulfhydrate and ferric chloride (0.4 mM) in 80% (v/v) ethanol solution in the molar ratio of 100 : 1 : 1, at pH 9.0. Adapted from ref. 107.

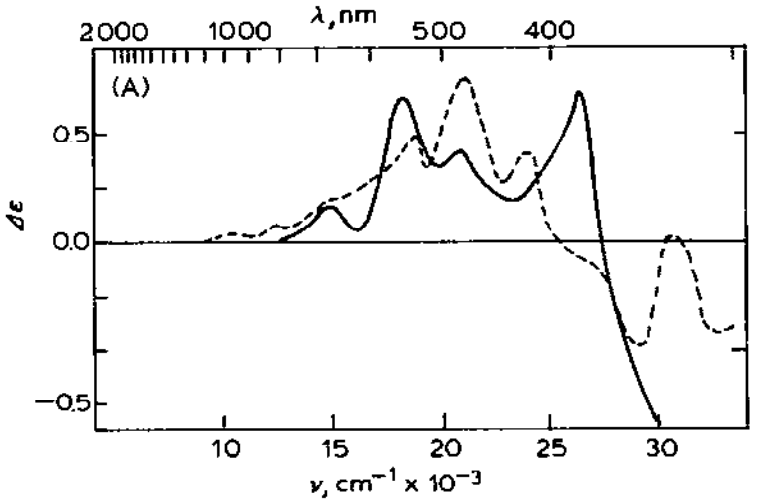
λ, nm
2000
1000
500
400
(A)
0.5
0.0
−0.5
Δε
10
15
20
25
30
ν, cm⁻¹ x 10⁻³

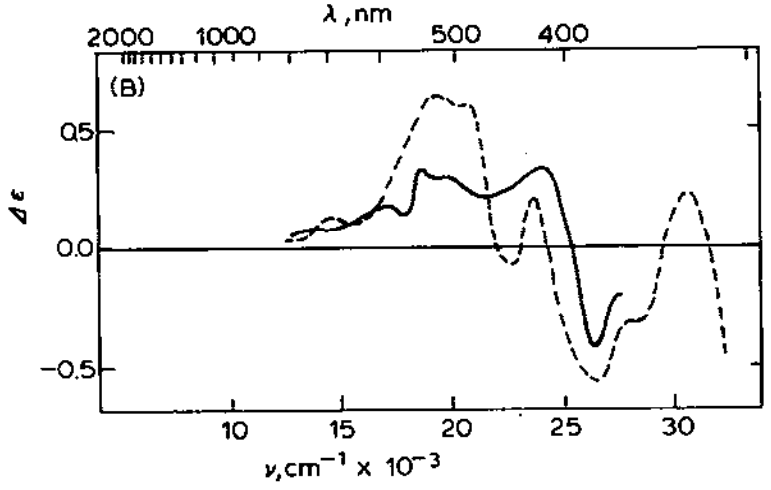
λ, nm
2000
1000
500
400
(B)
0.5
0.0
−0.5
Δε
10
15
20
25
30
ν, cm⁻¹ x 10⁻³

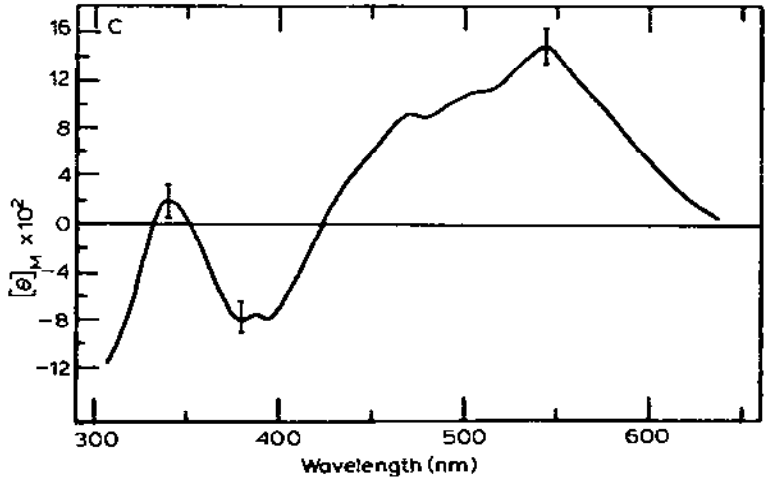
C
16
12
8
4
0
−4
−8
−12
[θ]M x10²
300
400
500
600
Wavelength (nm)

of the oxidized ferredoxin has an extra negative trough at ca. 450 nm and somewhat different relative intensities of the peaks that are in common with the spectrum of oxidized putidaredoxin. These slight differences could easily be accounted for by minor (less than 2%) contamination by a low-spin heme protein (vide infra). Additional peaks at ca. 800 and ca. 1000 nm are seen in the spectrum of oxidized putidaredoxin in the 800–1200 nm range.

The first MCD spectrum of an oxidized Fe_2S_2 center was reported by Sutherland et al. [111] in 1972. Except for the lack of the 310 nm trough, the spectrum is generally similar to that of oxidized putidaredoxin (Fig. 21A) although the features are poorly resolved and the data only extend to 625 nm. Unexpectedly, the intensities are about ten times larger than those in Fig. 21 or in any of the other Fe_2S_2 centers so far examined except xanthine oxidase (vide infra). The spectrum of oxidized spinach ferredoxin reported by Ulmer et al. [102] is very similar to that of putidaredoxin, including the intensities (after conversion to common units, $\Delta\epsilon$ $Tesla^{-1}$). Insufficiently absorbing samples likely caused Ulmer et al. [102] not to obtain spectra for oxidized putidaredoxin and adrenodoxin. The latter has still not been examined by MCD in its oxidized state. Thomson et al. have also reported the room temperature spectrum of oxidized *Spirulina maxima* ferredoxin [112]; which is in close agreement with Fig. 21B. No major differences are seen at 18 K, either in shape or intensity, compared to the other spectra discussed above [112]. The lack of intensity change at low temperature is consistent with a diamagnetic spin-paired ($S = 0$) ground state as suggested by magnetic susceptibility [118].

The case of xanthine oxidase warrants special attention. Xanthine oxidase is a complex two subunit protein with molybdenum, flavin and iron–sulfur cofactors present [119]. The protein has a molecular weight of ca. 280000 with 8 irons, 8 inorganic sulfides, 2 molybdenums and 2 flavins [116,117]. Obviously the iron and sulfide could be present in two Fe_4S_4, four Fe_2S_2 or in one Fe_4S_4 and two Fe_2S_2 units. The initial study by Bayer et al. [115] in 1971 shows a very poorly resolved spectrum with a broad positive band at 520 nm and a broad negative band at 375 nm. These features were attributed to the iron–sulfur component because flavin and molybdenum chromophores that were examined gave MCD effects an order of magnitude less intense. However, since this study was published before the first MCD was reported on spinach ferredoxin [111], no conclusions about the identity of the iron–sulfur components of xanthine oxidase could be reached. Bayer et al. did, however, suggest that the protein had Fe_2S_2 centers present based on a comparison of the CD spectrum of the protein to that of spinach ferredoxin. In 1973, Ulmer et al. [102] reported that the MCD spectrum of xanthine oxidase was very similar to that of spinach ferredoxin obtained in their laboratory. Although they did not actually show their spectrum of

xanthine oxidase, they did speculate that it likely had an analogous electronic structure to spinach ferredoxin, implying a similar Fe_2S_2 cluster composition. Indeed, in 1978, Holm and co-workers [116,117] examined xanthine oxidase by the technique of core extrusion and obtained strong evidence for the presence of Fe_2S_2 centers in the protein, just as predicted from comparison of the MCD spectra of xanthine oxidase and spinach ferredoxin [100].

Four potential oxidized Fe_2S_2 model complexes have been examined by Hatano and co-workers [107]. The MCD spectrum of a 1,4-butanedithiol : ferric iron : sulfide adduct (Fig. 21C) does a reasonable job of matching the spectrum of oxidized putidaredoxin (Fig. 21A) both in terms of overall intensity and band position, although not in terms of relative intensity of the observed transitions. The *o*-xylyl-α,α'-dithiol : ferric iron : sulfide adduct, previously synthesized by Holm and co-workers [120,121] as an oxidized Fe_2S_2 model, was also studied by the Hatano group who reported an absorption spectrum of the complex [107] that was essentially identical to that previously published [120,121]. However, its MCD spectrum did not match that of oxidized putidaredoxin as well as that of the 1,4-butanedithiol complex. A third model complex studied by the Hatano group, prepared from β-mercaptoethanol, ferric chloride and sulfide gave rise to an MCD spectrum that was nearly identical to the spectrum of oxidized putidaredoxin in the 400–650 nm region but was somewhat different below 400 nm. Finally, a presumably analogous complex formed from 1,6-hexanedithiol, ferric chloride and sulfide gave an MCD spectrum that was very different from the target spectrum. As all four model complexes studied by Hatano and co-workers displayed very similar absorption spectra, the variability of their MCD spectra clearly indicates the increased utility of this technique for characterizing the electronic structures of such clusters and, ultimately, for determining which adducts are the best models for the protein bound oxidized Fe_2S_2 unit.

Sutherland et al. [111] also reported the room temperature MCD spectrum of reduced spinach ferredoxin from 250–625 nm. Above 300 nm, four MCD features were seen that can be associated with the iron–sulfur clusters: a negative shoulder at ca. 320 nm and three broad peaks of roughly equal intensity at ca. 360, ca. 410 and ca. 520 nm. Once again, the overall intensities for their MCD spectrum of the reduced ferredoxin are about a factor of ten greater than reported by others [102,113] for related reduced Fe_2S_2-containing systems. For example, Stephens et al. [113] studied reduced putidaredoxin and reduced *Spirulina maxima* ferredoxin. The spectrum of reduced putidaredoxin (Fig. 21B) is generally similar to, although somewhat red-shifted from, that of spinach ferredoxin [111]. The negative band is at less than 333 nm with the analogous positive features at ca. 380, ca. 480 and

ca. 550 nm. Another weaker positive band is seen at ca. 675 nm outside the range examined by Sutherland et al. [111]. As indicated above, the sample of *Spirulina maxima* ferredoxin examined by Stephens et al. [113] may have been contaminated by a very small (< 2%) low-spin heme impurity. In the spectrum of the reduced protein (Fig. 21B), this is suggested by the derivative shaped feature superimposed on a sloping signal and centered at 550 nm, exactly where reduced low-spin hemes usually have their greatest (derivative shaped) MCD intensity. Otherwise, the spectrum follows the same pattern as just discussed for the other two examples of reduced Fe_2S_2 centers with a further red shift. For this case, the negative band in the near-UV is seen at ca. 380 nm and the positive bands are at ca. 419, ca. 510, ca. 540, ca. 590 and ca. 750 nm. If a low-spin heme is in fact present, then the features at ca. 540 and ca. 590 nm would be replaced by a single positive band at ca. 570 nm, thus fitting more exactly the one negative, four positive band patterns seen for reduced putidaredoxin (Fig. 21A) and reduced spinach ferredoxin [111] (in the latter case, only three positive bands were seen due to the narrower range of the study).

In light of the overall similarities seen and just discussed for three reduced Fe_2S_2 systems, the room temperature spectrum of reduced spinach ferredoxin published by Ulmer et al. [102] is noticeably different and likely in error. In this case only, a negative MCD transition is seen at ca. 455 nm. The other extrema (negative at ca. 380 and positive at ca. 405 and 555 nm) are somewhat similar to those observed for the other reduced Fe_2S_2 proteins.

Thomson and co-workers [112,114] have examined the MCD of reduced spinach ferredoxin, *Spirulina maxima* ferredoxin and adrenodoxin over a wide temperature range. Their initial study at low temperature reported the spectra of the three proteins at 20, 6.5 and 6.5 K, respectively [112]. Considerable sharpening and intensification (ca. $\times 10$) of the features observed at room temperature [111,113] for the two ferredoxins was seen; the resulting low temperature spectra were quite similar to each other. The 6.5 K MCD spectrum of reduced adrenodoxin was somewhat different from those of the two ferredoxins both in band intensities and in the red shifted location of the MCD features. The authors attributed the observed shifts in the spectrum of reduced adrenodoxin to known differences in the exchange coupling between the two metals [118,122] and postulated that this reflected changes in the iron to iron distance [105,112].

More recently, Thomson and co-workers [114] have reported a variable low temperature and variable field study of *Spirulina maxima* ferredoxin. By examining the intensity of various transitions as a function of increasing magnetic field and decreasing temperature, magnetization curves were determined. As discussed in Section B, magnetization curves can be used to determine ground state g factors. In this way g values of $g_{\parallel} = 2.05$ and

$g_\perp = 1.93$ were calculated. These values are well within the range usually seen for reduced Fe_2S_2 proteins [123] and are consistent with an $S = 1/2$ ground state such as would be expected for an antiferromagnetically coupled high-spin Fe(II) : high-spin Fe(III) pair. EPR and Mössbauer studies also suggest an $S = 1/2$ ground state [123].

The most obvious area for future study of Fe_2S_2 clusters with MCD spectroscopy will be the examination of model complexes for the reduced sites. The characteristic spectra and, in particular, temperature dependence including magnetization curves will provide an exacting test for the integrity of such models. It will also be important to examine oxidized Fe_2S_2 proteins from other sources and to re-examine spinach ferredoxin to clarify the drastic discrepancies seen in the room temperature data from two laboratories [102,121]. In particular, the concept developed by Thomson and co-workers [105,112] based on their low temperature study of reduced adrenodoxin that there are two types of Fe_2S_2 clusters with subtle but spectroscopically detectable differences needs to be tested further. Most importantly, oxidized adrenodoxin needs to be studied at ambient as well as low temperatures in order to compare it to the other oxidized Fe_2S_2 systems. The only previously reported attempt to measure the MCD spectrum of oxidized adrenodoxin was unsuccessful [102].

(iii) Four-iron iron–sulfur proteins and model systems

As is now well established [99,124], four-iron iron–sulfur clusters in proteins can exist in three physiologically relevant oxidation states. Electron transfer proteins containing this type of metal center fall into two categories depending on whether they normally exist in the highest two or lowest two of these three oxidation states. The most well studied protein in the first category is the high potential iron protein (HIPIP) from *Chromatium*. Numerous low potential ferredoxins are known in the second category. Oxidized HIPIP is paramagnetic and has an iron–sulfur cluster composition of $[Fe_4S_4(S\text{–}Cys)_4]^-$. This oxidation state, which corresponds formally to a cluster with three ferric and one ferrous iron centers, will be designated C^-. Addition of one electron to oxidized HIPIP produces the diamagnetic C^{2-} state. This cluster oxidation state is also found in the oxidized low potential ferredoxins. Further reduction of C^{2-} by one electron yields the paramagnetic, reduced low potential C^{3-} state. Our current understanding of the structural properties of the four-iron iron–sulfur clusters has resulted primarily from X-ray crystallographic studies [124] and from the elegant work of Holm and co-workers [125] who have prepared synthetic analogs for these clusters.

Following an initial survey study by Ulmer et al. [102] and a very brief

report by Mason and Zubieta [126], the most extensive application of MCD spectroscopy to the examination of this class of iron–sulfur proteins has come from the laboratories of Thomson and co-workers [113,114,127]. MCD spectra of oxidized and reduced HIPIP, *Bacillus stearothermophilus* ferredoxin and of a synthetic analog of the C^{2-} state have been measured at ambient temperature over the 300–2000 nm range [113,127]. The same protein states have also been investigated over the 300–800 nm range as a function of temperature between 1.5 and 50 K and magnetic field up to 5.3 Tesla in order to obtain magnetization curves (vide supra).

The most obvious and striking observation about the MCD spectra of all three four-iron iron–sulfur cluster oxidation states is that all are entirely positive in sign from 300–2000 nm at ambient temperature. This is readily seen in Fig. 22 where the spectra of oxidized HIPIP (Fig. 22A), of reduced HIPIP, oxidized *Clostridium pasteurianum* ferredoxin and the C^{2-} cluster model (Fig. 22B) and of the reduced ferredoxin (Fig. 22C) are displayed [127]. At ultra-low temperature, negative features are observed [114] in each case so far examined; in addition the spectral features sharpen and, in some cases, intensify dramatically due to the presence of MCD *C* terms. The overall intensities of the spectra of the C^{-}, C^{2-} and C^{3-} clusters are comparable at ambient temperature and, as in the case of the two-iron iron–sulfur proteins, are about a factor of ten less than the one-iron rubredoxin case.

The ambient temperature MCD spectrum of oxidized HIPIP (Fig. 22A) has six broad bands (320, 390, 510, ca. 590 (shoulder), 950 and 1150 nm) [113,127]. Dramatic changes in intensity occur in the spectrum upon cooling to 1.5 K [112] because of the paramagnetic nature of the C^{-} cluster [99]. From the shape and form of the magnetization curve obtained from data at 1–5 Tesla and 1.5–47.0 K, it is possible to calculate the ground state *g* values. The computed values [114] of $g_{\parallel} = 2.12$ and $g_{\perp} = 2.4$ are identical to the values determined directly by EPR spectroscopy [128]. The low temperature spectrum is also noticeably more detailed, with negative as well as positive extrema observed. Nine transitions are apparent between 300 and 700 nm at 1.5 K where only four are observed at ambient temperature over the same spectral range. Clearly the broad bands observed in the room temperature spectrum actually consist of numerous overlapping transitions that are much better resolved at very low temperature.

The MCD spectrum of reduced HIPIP at ambient temperature (Fig. 22B) is of comparable intensity to that of the oxidized protein (Fig. 22A) and consists of seven broad positive maxima (385, 460, 595, 680, 780, 1200 and ca. 1500 (shoulder)) [113,127] between about 330 and 2000 nm. In fact, the distinctions between the two spectra are less than expected following the change in oxidation state of the cluster. The only change that occurs in the

spectrum upon cooling to 4.2 K is the sharpening of the bands with concomitant resolution of both of the 385 and 460 nm peaks into two features [114]. The low temperature spectrum also extends to 300 nm and

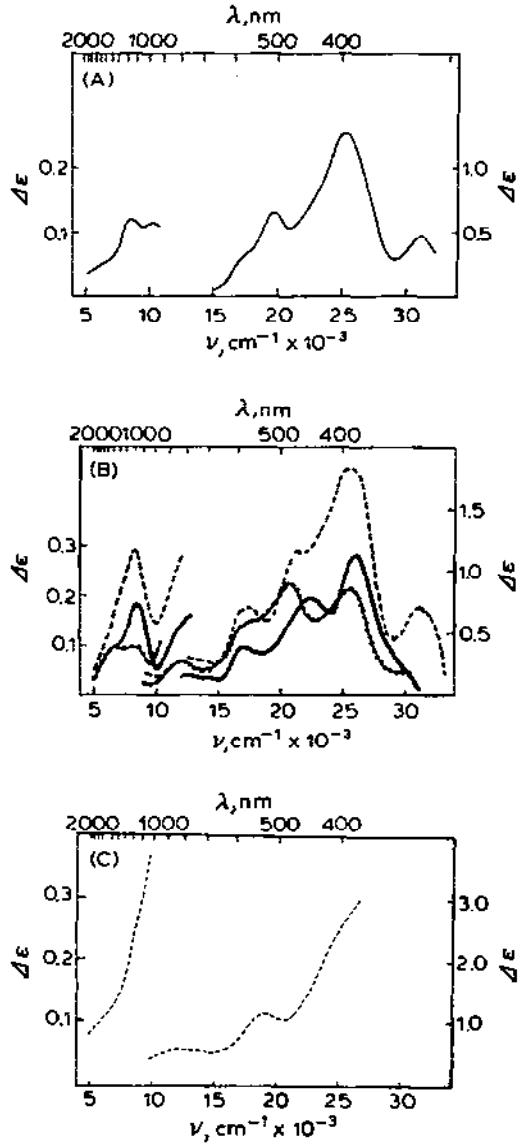

Fig. 22. (A) MCD spectrum (normalized to 1 Tesla) of oxidized *Chromatium* HIPIP. Adapted from ref. 127. (B) MCD spectra (normalized to 1 Tesla) of: reduced *Chromatium* HIPIP (———); oxidized *Clostridium pasteurianum* ferredoxin (- - - - -); and $[N(C_2H_5)_4]_2[Fe_4S_4(SCH_2C_6H_5)_4]$ (in dimethylformamide) (·—·—·). Adapted from ref. 127. (C) MCD spectrum (normalized to 1 Tesla) of reduced *Clostridium pasteurianum* ferredoxin (- - - - -). Adapted from ref. 127.

includes a negative band at 315 nm. The near-IR region of the spectrum was not measured at low temperature. The complete lack of intensity change for the spectrum of reduced HIPIP upon cooling confirms the diamagnetic nature of its ground state and attests to the homogeneity of the sample; previous bulk susceptibility studies of this protein state were complicated by the apparent presence of a minor paramagnetic impurity [129]. Thus the use of low temperatures dramatically distinguishes the MCD properties of oxidized and reduced HIPIP, the former is temperature dependent due to *C* terms and the latter is not.

The MCD spectrum of oxidized *Clostridial* ferredoxin should be very similar to that of reduced HIPIP because both are thought to be C^{2-} clusters [99,124] (Fig. 22B). This is true in a general sense although differences are seen between the two spectra; an extra band is seen at ca. 330 nm in the spectrum of the ferredoxin and only one very broad band between 650 and 1000 nm where two features are seen in the spectrum of reduced HIPIP. A likely explanation for these small differences is provided in the low temperature work on oxidized *Clostridial* ferredoxin [114]. Instead of finding the MCD spectrum to be temperature independent as was found for reduced HIPIP and as would be expected for the diamagnetic, oxidized, low-potential ferredoxin, a marked intensity increase was observed upon lowering the temperature below 50 K. However, the magnitude of the increase indicated that only about 10% of the sample was responding to the lowered temperature. In other words, the sample of oxidized ferredoxin was contaminated with a paramagnetic impurity whose MCD spectrum was temperature dependent and would, in fact, dominate the overall spectrum at 1.95 K. This finding was in keeping with the consistent observation in several laboratories that oxidized *Clostridial* ferredoxin displays a weak EPR spectrum [114,130]. As will be discussed later, this paramagnetic impurity is not the C^{-} four-iron cluster but instead is a new type of iron–sulfur cluster with only three irons.

The only four-iron iron–sulfur model complex that has been examined so far was a C^{2-} cluster studied at room temperature by Stephens et al. [113] (Fig. 22B). As can be seen, the spectrum of the model matches those of reduced HIPIP and of oxidized *Clostridial* ferredoxin reasonably well. Unfortunately, the spectrum has not been obtained at low temperature to see if it is free of paramagnetic impurities. Similar model complexes do not display EPR spectra [115].

Stephens et al. [113,127] have also examined oxidized *Bacillus sterothermophilus* ferredoxin by MCD spectroscopy and obtained a spectrum at ambient temperature that is quite similar to that of oxidized *Clostridial* ferrodoxin. The first MCD spectrum of oxidized *Clostridial* ferredoxin (300–600 nm) was published by Ulmer et al. [102] and is reasonably similar to that displayed in Fig. 22. These authors also examined reduced *Clostridial*

ferredoxin and only saw an increasing signal with decreasing wavelength over the 400–600 nm range. MCD spectra of *Micrococcus lactilyticus* ferredoxin, although limited in scope to the 350–500 nm region, are consistent with that described herein for *Clostridial* ferredoxin [126].

Reduced *Clostridial* ferredoxin has also been examined at ambient temperature with MCD spectroscopy over the 380–2000 nm wavelength range (Fig. 22C). Two very broad peaks are observed at 540 and 800 nm (see also ref. 112). The signal is sharply increasing at 380 nm where the data stops; presumably a peak would be observed at between 350 and 380 nm, as is seen for reduced *M. lactilyticus* ferredoxin [126]. In the near-IR region the signal decreases with increasing wavelength without a clear peak being observed. Similar data over the same wavelength range were reported for reduced *Bacillus stearothermophilus* ferredoxin except that a shoulder is clearly resolved in the near-IR region at ca. 1150 nm [113,127].

As with oxidized HIPIP, dramatic changes occur in the MCD spectrum of reduced *Clostridial* ferredoxin upon cooling to 1.55 K. Six positive and one negative maxima of substantially increased intensity are observed where just two were seen at ambient temperature over the 350–800 nm range. The intensity of the 540 nm maximum is over twenty times greater at 1.55 K than at room temperature [114]. Magnetization curves for reduced *Clostridial* ferredoxin permit calculation of g values of 1.90 ($g_\perp$) and 2.06 ($g_\parallel$). This is in close agreement with the literature values of 1.88, 1.92 and 2.06 [128]. The magnetization curves at 1.52 and 4.22 K are identical. Therefore at these temperatures the cluster is behaving as a simple Kramer's doublet $S = 1/2$ system. At 18.6 K, however, the magnetization curve is slightly steeper suggesting that some thermal population of low-lying electronic states is occurring [114]. EPR and magnetic susceptibility data on model complexes for the C^{3-} cluster also suggest that there may be low-lying excited states [131]. In contrast, the magnetization curves for oxidized HIPIP discussed earlier have the same shape from 1.50–47.0 K suggesting that no excited electronic states are populated over that range of temperature for the C^- state.

With this extensive and excellent work from the laboratories of Stephens and Thomson on HIPIP and on *Bacillus* and *Clostridial* ferredoxins, there does not appear to be much need for further MCD studies on these proteins. As suggested in ref. 114, a more thorough study of the magnetization of the C^{3-} cluster would help characterize the thermal population of low-lying excited states. Beyond that, the most obvious direction in which work on this topic should move is to the study of the model complexes for the C^-, C^{2-} and C^{3-} states [125], especially as a function of temperature. Indeed, reproduction of the detailed temperature dependent changes that are observed in the MCD spectra of the C^- and C^{3-} protein states may be the best

way to compare model complexes with intact proteins. Of course, it would also be useful to extend the existing data on the above-mentioned three proteins to some of the numerous other four-iron iron–sulfur proteins.

(iv) Three-iron iron–sulfur proteins and model systems

The most exciting discovery in the field of iron–sulfur proteins over the past few years has been the identification of three-iron iron–sulfur clusters in several proteins. The first convincing evidence for this new cluster type came from Mössbauer and EPR studies of the Münck group in collaboration with the Orme-Johnson group on *Azotobacter vinelandii* ferredoxin I [132]. The structure of that three-iron cluster has been determined crystallographically by Stout and co-workers [100,133]. The characteristic Mössbauer properties of the three-iron cluster have now been identified in several proteins including glutamate synthetase from *Azotobacter vinelandii* [132], aconitase from beef heart [134], ferredoxin II from *Desulfovibrio gigas* [135] and ferredoxins from *Thermus thermophilus* [136] and from *Methanosarcina barkeri* [137]. Several chapters in ref. 99 address the properties of the three-iron clusters [105,125,128,136–140]. In this section we will review the contribution that MCD spectroscopic studies, primarily by the Thomson group, have made to our understanding of three-iron clusters [141–143].

Although the first three-iron iron–sulfur cluster characterized was from *Azotobacter vinelandii*, the presence of an additional four-iron center in the same protein substantially complicated the analysis of the spectral properties of the new cluster. Consequently, the first MCD study of such a cluster was carried out on ferredoxin II from *Desulfovibrio gigas* [141], a protein that appears to contain only the three-iron unit [135]. The 4.22 K MCD spectrum of oxidized ferredoxin II is shown [141] in Fig. 23A overplotted with the spectrum of ferricyanide treated, "superoxidized" ferredoxin from *Clostridium pasteurianum* [142]; the reason for overplotting the two spectra lies in their close similarity, as will be discussed. In Fig. 23B, the low temperature MCD spectrum of reduced ferredoxin II is presented [141] overplotted (for the same reason as above) with the spectrum of dithionite re-reduced ferricyanide-oxidized *Clostridium pasteurianum* ferredoxin [142].

The Mössbauer and EPR studies of *Desulfovibrio gigas* ferredoxin II had established that the cluster was paramagnetic in both oxidation states with a $S = 1/2$ ground state in the EPR active oxidized form (nearly isotropic EPR, $g = 2.01$) and a ground state of unknown spin when reduced. The paramagnetic nature of both oxidation states of ferredoxin II was readily verified by Thomson et al. in their variable temperature MCD study [141]. Magnetization data very nicely fit a smooth curve calculated from an isotropic g value of 2.0 and $S = 1/2$. A plot of the MCD intensity vs. $1/T$ for

$T = 11.1–162.5$ K yielded a straight line only from 36–70 K. Above that temperature range there appeared to be thermally induced population of a low-lying excited state at about 80 cm^{-1} that led to diminished intensity.

As discussed by Thomson et al. [141], the low temperature MCD spectrum of oxidized ferredoxin II is quite complex with many more maxima than are present in the absorption spectrum. The less intense transitions in the 550–750 nm range were assigned to ligand field bands and the more intense features in the 250–550 nm region to charge transfer transitions from sulfur ligand orbitals to orbitals on the iron core atoms. The low temperature MCD spectrum of oxidized ferredoxin II (Fig. 23A) contrasts noticeably with that of oxidized HIPIP (Fig. 22A). The former spectrum has nearly an equal number of positive and negative maxima while the latter spectrum, even at low temperature [114], is nearly devoid of negative features. These differences may provide a useful way of distinguishing two oxidized iron–sulfur centers that have similar EPR characteristics [128].

The magnetization behavior of the reduced three-iron cluster was not nearly as simple as in the oxidized case [141]. Only at 1.530 and 1.995 K were the plots of MCD intensity vs. field strength superimposable. The plot is substantially steeper than for the $S = 1/2$ systems discussed above and the data points reach an asymptotic limit at the fields employed in the experiment, which means that the MCD signal is easily saturated. The steep magnetization curve could only be fitted in a reasonable fashion by assuming an axial ground state with $g_{\parallel} = 8.0$ and $g_{\perp} = 0.20$ and with $S = 2$. The

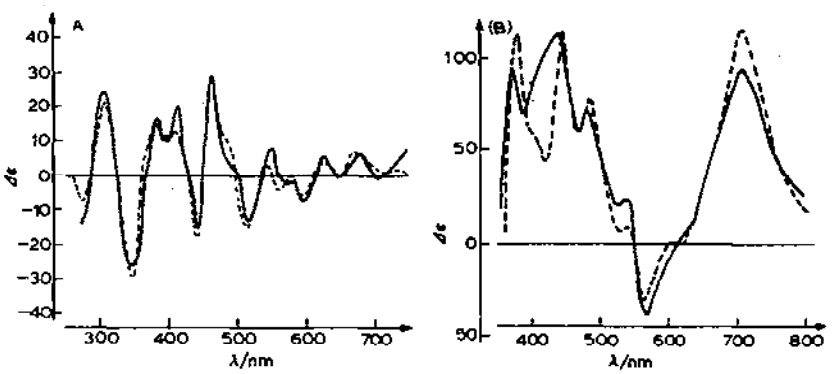

Fig. 23. (A) MCD spectra of ferricyanide-oxidized *Clostridium pasteurianum* ferredoxin (———) and oxidized ferredoxin II from *Desulfovibrio gigas* (- - - - -) at 4.215 K and 5.13 T. The Δε scale refers only to the spectrum of ferredoxin II. The spectra have been normalized at 462 nm. From ref. 142. (B) MCD spectra of dithionite-reduced, ferricyanide-oxidized *Clostridium pasteurianum* ferredoxin (———) and dithionite-reduced ferredoxin II from *Desulfovibrio gigas* at 4.215 K and 5. 13 T. The Δε scale refers only to the spectrum of ferredoxin II. The spectra have been normalized at 500 nm. From ref. 142.

Mössbauer data on reduced ferredoxin II was best fitted with an integer spin greater than or equal to one. Above 2 K, the magnetization curves begin to fall off and probably would approach a lower asymptotic limit. Thus, at higher temperatures, low-lying excited states can be populated and the resulting MCD signals are of lower intensity. Clearly, its unique magnetization curve distinguishes the reduced three-iron center from all other iron–sulfur clusters. The actual low temperature MCD spectrum of reduced ferredoxin II is much simpler than that of the oxidized state (Fig. 23B) and, like the spectra of the four-iron oxidation states, is predominantly positive in sign.

With the low temperature MCD properties of the three-iron iron–sulfur cluster in ferredoxin II as a basis, Thomson et al. extended their work to the peculiar properties of ferricyanide treated, "superoxidized," low potential ferredoxin [142]. Treatment of oxidized *Clostridial* ferredoxin with ferricyanide was known to lead to a derivative with a large isotropic EPR signal at 2.01 [130]. Although this EPR signal is not identical to that of oxidized HIPIP, it was nonetheless concluded that the ferricyanide treated derivative was a superoxidized or C^- cluster. Comparison of the characteristic low temperature MCD spectra of the fully oxidized three (Fig. 23A) and four [114] iron centers, however, suggests otherwise [142]. Clearly, ferricyanide treatment of *Clostridial* ferredoxin leads to loss of an iron and formation of the oxidized three-iron cluster. Furthermore, reduction of the ferricyanide treated protein does not restore the reduced, C^{3-}, cluster. Instead, the dithionite re-reduced, ferricyanide treated ferredoxin has a spectrum that is very similar to that of a reduced three-iron center (Fig. 23B). This conversion of the four-iron cluster of a low potential ferredoxin into a three-iron center by such treatment has been verified now in several cases [134,144–147].

Aconitase is a special case among iron–sulfur proteins. As discussed by Piszkiewicz et al. [143], aconitase has been studied by several chemical and spectroscopic techniques without a consensus being reached about the identity of its iron–sulfur cluster. Most recently, a thorough study with Mössbauer and EPR spectroscopy led to the conclusion that aconitase has interconverting three- and four-iron centers [134]. Clearly the application of low temperature MCD spectroscopy will help solve this dilemma owing to the diagnostic and distinguishable properties of each possible three- and four-iron cluster. The published MCD study, unfortunately, is inconclusive because the data are noisy and were measured at room temperature [143]; no room temperature MCD spectra of the three-iron clusters have yet been published.

Much remains to be done with MCD spectroscopy in the study of three-iron iron–sulfur clusters. As mentioned earlier, numerous proteins, including aconitase, are now thought to contain the three-iron center. The

application of MCD spectroscopy, particularly at low temperature following the model of Thomson, will help resolve this issue. The recent success of the Holm laboratory in preparing trinuclear iron thiolate complexes [148] suggests that synthetic analogs of the protein site will soon follow. MCD spectroscopy will be a sensitive tool to use in characterizing such systems. Finally, recent extended X-ray absorption fine structure examination of *Desulfovibrio gigas* ferredoxin II [139,149] has revealed substantial differences in the iron–iron separation from that observed by X-ray crystallography for the three-iron unit in *Azotobacter vinelandii* [133,138]. The authors tentatively concluded that there may be more structural variability in the three-iron case than is seen in the two- and four-iron systems. Such structural variability would certainly lead to spectroscopic distinctions that should be readily observed by MCD spectroscopy.

(v) Iron–sulfur proteins: overview

In the preceding portions of this section we have generally considered each of the basic types of iron–sulfur proteins independently and have not attempted to directly compare the MCD properties of the different classes with each other to a very large extent. In this portion, we will briefly do such a comparison focusing particularly on how one could use MCD spectroscopy to classify an iron–sulfur center of unknown identity. First, however, we will consider the advantages MCD spectroscopy has over other techniques in characterizing iron–sulfur centers.

For a number of reasons, MCD spectroscopy is a particularly useful technique for characterizing the electronic structures of iron–sulfur centers in proteins. In comparison to UV–visible absorption spectroscopy and like CD spectroscopy, the MCD spectra of particular iron–sulfur chromophores are substantially more featured and therefore provide a more diagnostic fingerprint to use in assigning structure (see ref. 113, for example). Furthermore, MCD is much less sensitive to the environmental factors that dramatically effect CD spectra. Consequently, one can directly compare the MCD spectra of a certain iron–sulfur cluster in a particular oxidation state from two different proteins or even from a model complex and, if the structures are indeed comparable, the MCD spectra should be nearly the same. In comparison to EPR spectroscopy, MCD spectra can be obtained for all oxidation states of the iron–sulfur sites, not just the non-integer spin paramagnetic cases. Furthermore, although the use of low temperature leads to substantially more detailed results, MCD can be measured at ambient temperature and significant information obtained.

As has been elegantly demonstrated by Thomson and co-workers [105], the use of low temperatures adds a new dimension to the study of iron–sulfur

chromophores by MCD spectroscopy. As outlined earlier in this review, MCD spectra of paramagnetic species measured at very low temperature have substantially enhanced signal intensity and increased spectral detail. Further, by plotting signal intensity versus magnetic field, a magnetization curve is obtained that is characteristic of a particular ground state and spin state. Ground state g values can be calculated from the magnetization curve. The steepness of the magnetization increase, the degree to which the signal can be saturated at available magnetic fields and the relationship of magnetization curves at different temperatures (all curves superimposable or arranged in a "nested" fashion) are all additional parameters that can be used to determine the electronic properties of the iron center [105]. In addition, it is possible to detect the thermal population of low lying excited states (e.g., produced by zero-field splitting or magnetic interactions) and to estimate the energy gap between such states and the ground state.

Another direction in which MCD spectroscopy has been applied is the study of iron–sulfur chromophores in the near-infrared region. This development has been used most effectively by Stephens and co-workers [43,127,150,151]; its utility will be discussed below.

MCD spectroscopy can be readily used to identify iron–sulfur cluster types in proteins of unknown composition. This is true for the iron–sulfur centers containing one to four irons per unit when low temperature MCD is employed. Since no well resolved room temperature MCD have been published for the proteins that are best established as containing three-iron clusters, it is only possible to state that one, two and four iron centers in proteins can be distinguished at room temperature. As any such attempt to identify the iron–sulfur center in an uncharacterized protein would likely involve examination of both the oxidized and reduced forms, it is really a pair of spectra that need to be considered for each iron–sulfur type site. Examination of the spectra measured at room temperature of the one-, two- and four-iron centers (Figs. 20–22) reveals the following diagnostic criteria that can be used for identification of iron–sulfur type. (1) The spectra of oxidized and reduced rubredoxin are clearly distinct from the rest both in terms of their relative intensity (tenfold greater) and their characteristic shapes (oxidized: multiband pattern of alternating sign; reduced: no features above 400 nm). (2) The spectra of the oxidized and reduced two-iron iron–sulfur center lack measurable features in the near-IR beyond 1000 nm and have several positive bands above about 400 nm in the oxidized case (about 375 nm in the reduced case) with negative features below those wavelengths. (3) The three oxidation states of the four-iron clusters each have distinct features above 1000 nm and display only positive peaks above about 300 nm. (4) The distinctions between the MCD spectra of the C^- and C^{2-} clusters are relatively small but the C^{3-} cluster has fewer bands and

only decreasing intensity above 1000 nm without a separate maximum; thus, the C^{3-}, C^{2-} pair can be distinguished from the C^{2-}, C^{-} pair based on the properties of the C^{3-} cluster. In this fashion, Stephens et al. [150] have identified the iron protein in nitrogenase as containing the low potential, four-iron iron–sulfur cluster type. In addition, Ulmer et al. [102] were able to predict that the iron–sulfur centers in xanthine oxidase are of the two-iron class, a prediction borne out by core extrusion experiments [116,117].

At low temperature, the increased complexity and intensity of the MCD spectra of paramagnetic iron–sulfur centers coupled with the use of magnetization curves makes identification of the iron–sulfur type even more straightforward [105]. For example, only the one-iron and three-iron centers display temperature dependent MCD spectra in both oxidized and reduced states; however, the shapes of the low temperature spectra allow the two classes to be distinguished. Magnetization curves have not yet been published for the rubredoxin case. Both the two-iron and low potential four-iron clusters display temperature dependent MCD spectra when reduced that are readily distinguished due to their shape. Finally, the high potential four-iron cluster is unique in that it displays temperature dependent MCD spectra when oxidized but not when reduced. Clearly, low temperature MCD spectroscopy can be definitively used for the identification of iron–sulfur type. As discussed above, room temperature data can also be used for the same purpose and while the results may not be quite as conclusive as with the low temperature data, the experimental set-up for work at room temperature is substantially simpler.

(vi) Nitrogenase

One of the more intriguing problems facing the field of bioinorganic chemistry at the present time is the determination of the active-site structure and mechanism of action of an enzyme complex known as nitrogenase that consists of two protein components, one called the iron (Fe) protein and the other called the molybdenum–iron (MoFe) protein [152–154]. This metalloenzyme system is able to reduce dinitrogen by six electrons to form two molecules of ammonia; several other unsaturated molecules can also be reduced. The Fe and MoFe proteins are readily separable and therefore have been individually examined. In addition, an iron molybdenum cofactor (FeMoCo) has been separated from the FeMo protein; the cofactor contains all of the molybdenum in the MoFe protein and some of the iron. The Fe and FeMo proteins have been isolated from numerous sources including *Azotobacter vinelandii* (*Av*), *Clostridium pasteurianum* (*Cp*) and *Klebsiella pneumoniae* (*Kp*). The MoFe proteins from each of these sources are referred to as *Av*1, *Cp*1 and *Kp*1 and the Fe proteins as *Av*2, *Cp*2 and *Kp*2.

Iron protein

The only study of the iron protein of nitrogenase using MCD spectroscopy is that by Stephens et al. [150] who examined the Fe protein derived from *A. vinelandii* (*Av*2) and from *K. pneumoniae* (*Kp*2) at ambient temperature. Both proteins were examined in their dithionite reduced forms and *Av*2 was studied in a post-steady-state oxidized form. Comparison of the spectrum of reduced *Av*2 with that of the reduced (C^{3-}) four-iron iron–sulfur ferredoxin from *C. pasteurianum* (Fig. 22C) led to the conclusion that both proteins have the same cluster type, thus placing the Fe protein of nitrogenase in the four-iron ferredoxin class [150]. Further support for this assignment comes from comparison of the MCD spectrum of the post-steady-state oxidized *Av*2 to that of oxidized *Clostridial* ferredoxin (Fig. 22B). Both proteins have characteristic near-IR MCD bands at ca. 1200 nm and ca. 850–900 nm. Unfortunately, the rest of the MCD spectrum of oxidized *Av*2 is not very well resolved and so additional comparisons are difficult. The MCD spectrum of oxidized *Av*2 does, however, go negative below ca. 380 nm, in contrast to the spectrum of oxidized *Clostridial* ferredoxin.

Thus the MCD study by Stephens et al. [150] of the Fe proteins of nitrogenase provides a prime example of how MCD spectroscopy can be used to delineate structural possibilities among iron–sulfur types. Of course, as stated in Section F(v), the conclusions reached would be strengthened by further studies at low temperature [105]. Nonetheless, the MCD data on the Fe protein of nitrogenase are more consistent with the presence of a four-iron iron–sulfur cluster than with clusters of the two-iron type.

Iron–molybdenum protein

The greatest challenge in the study of nitrogenase is the MoFe protein. With approximately thirty iron atoms, a comparable number of inorganic sulfides and two molybdenum atoms, there is much to be learned. A further complication arises from the observation from Mössbauer studies of the MoFe protein that at least three different types of iron are present [155]. One type belongs to a dissociable iron–molybdenum cofactor (FeMoCo, M center) having 6–8 iron atoms and 4–6 inorganic sulfides per molybdenum [151,156]; the other types (P and S centers) are believed to be associated with iron–sulfur clusters [151,157–160]. Stephens et al. [150,151] were the first to examine the MoFe protein (from *A. vinelandii* and *K. pneumoniae*) using MCD spectroscopy. While their studies were carried out at room temperature, they did cover a wide wavelength range (300–2000 nm). Several important conclusions were drawn from examination of these MCD spectra and comparison of them to the spectra of known four-iron iron–sulfur proteins in all three available oxidation states: C^{-}, C^{2-} and C^{3-}. First of all, close structural correspondence is suggested for reduced *Av*1 and *Kp*1

based upon their nearly identical MCD properties. Further, while the spectra of reduced *Av*1 and *Kp*1 are most similar to that of a reduced low potential ferredoxin (C^{3-}) such as from *C. pasteurianum* (Fig. 22C), important differences exist. Examination of the anisotropy ratio ($\Delta\epsilon_M/\epsilon$) and of the ratio of MCD intensities of the spectra of the two proteins further supports that conclusion [151]. In particular, the MCD intensity for reduced *Av*1 diminishes to essentially zero at 7000 cm^{-1} (ca. 1400 nm), whereas all three accessible oxidation states of four-iron iron–sulfur clusters exhibit appreciable intensity in the 5000–7000 cm^{-1} range (ca. 1400–2000 nm). To rule out the possibility that reduced *Av*1 is a super-reduced (C^{4-}) low potential ferredoxin, an oxidized preparation of *Av*1 was investigated. In constrast to what would be expected for an oxidized form of a C^{4-} cluster, no MCD intensity is observed below 7000 cm^{-1}.

One major limitation of the room temperature study of the reduced MoFe protein is that the observed spectrum represents the sum of contributions from all of the different iron sites. The selective MCD intensity enhancement of paramagnetic chromophores upon lowering the temperature allows such centers to be examined in the presence of diamagnetic ones. This has been done by Thomson and co-workers [157] who have carried out a variable temperature MCD study of reduced and oxidized *Kp*1. From extensive Mössbauer studies of dithionite-reduced and thionine-oxidized MoFe protein, it appears that only one type of paramagnetic center having spin $S = 3/2$ exists in the reduced form and that an unusual, EPR silent, paramagnetic site exists in the oxidized state [158–160]. In the reduced form, the paramagnetic species appear to be associated with the iron–molybdenum center (M center). In this state, the other iron atoms (P and S centers) are diamagnetic. Upon oxidation, the M center becomes diamagnetic and the irons in the P centers become paramagnetic. There appear to be only two iron atoms of the S type and they do not change magnetic properties upon oxidation state changes. As Thomson et al. have recently reviewed their low temperature MCD studies of nitrogenase [105], only the major conclusions of that work will be discussed here.

As mentioned above, the only paramagnetic site in the reduced MoFe protein is believed to be the M center (FeMoCo) and so it is the MCD spectrum of this cluster that dominates at low temperature (20 K or less) [157]. Nested MCD magnetization curves were obtained, pointing to a complex magnetic ground state; in addition, at 1.54 K, the M center cannot be completely saturated even at 5.1 T. Nonetheless, the magnetization properties are quite consistent with the known properties of the M center from EPR and Mössbauer spectroscopy and also provide an excellent fingerprint of that center to use in evaluating the extracted iron–molybdenum cofactor (M center) and for diagnosis of any iron–molybdenum cluster model complexes.

The thionine-oxidized MoFe protein is thought to have paramagnetic centers (P centers) that are comprised of iron and sulfide without molybdenum. In principal, therefore, they could be conventional iron–sulfur clusters such as found in the ferredoxins. Several lines of evidence argue against that conclusion. Mössbauer spectroscopy suggests that the irons in the P center are not all equivalent and are present in two forms in a three to one ratio [159]. Furthermore, as presented above, the room temperature MCD studies of Stephens et al. [150,151] are inconsistent with the presence of a standard iron–sulfur cluster in the MoFe protein. This conclusion is convincingly confirmed through the use of low temperature MCD spectroscopy [157]. In fact, the MCD properties of the thionine-oxidized MoFe protein are completely unique among all known iron–sulfur centers [105]. Because the major bands in the spectrum respond to temperature and field in an identical fashion, it is clear that they all originate from one metal center. The most striking feature of the magnetization curve is that at 1.54 K, the P center becomes 90% magnetized at a field of only 1.5 T. These unusual magnetization properties of the thionine-oxidized protein distinguish it relative to the reduced form even though the low temperature MCD spectra of the two states are somewhat similar. Once again, it is clear from the unique magnetization curve for the oxidized protein that the P centers are not conventional iron–sulfur clusters such as have been previously examined at low temperature [105].

No positive evidence for the identity of the remaining irons in the MoFe protein, the S centers, has come from the MCD work described here. However, the lack of any appreciable contribution to the low temperature MCD spectra of both the oxidized and reduced MoFe protein requires that the S centers remain diamagnetic in both oxidation forms of the protein. As there are two S-type irons in the protein, and since either an oxidized or reduced rubredoxin type iron or a reduced two iron iron–sulfur type iron would display a noticeable temperature-dependent MCD spectrum, this leaves only the oxidized two-iron iron–sulfur center as a possibility among conventional iron–sulfur centers. Of course, it is entirely possible that the S center represents a new type of iron site not found in other known non-heme iron proteins.

(vii) Other non-heme iron proteins

While the great majority of the investigations of non-heme iron proteins with MCD spectroscopy have focused on the iron–sulfur proteins, a few additional proteins have also been examined. In their initial survey of the MCD of many non-heme iron metalloproteins, Ulmer et al. [102] examined ferric transferrin and conalbumin as well as oxy- and met-hemerythrin.

Much more recently, Bull and Ballou [161] have examined native, substrate-bound and product-bound protocatechuate 3,4-dioxygenase. None of these studies has been particularly extensive; the data were generally obtained at room temperature and were only measured in the UV–visible wavelength range (300–600 nm [102] and 300–800 nm [161]). Consequently, these data really serve only as a beginning to a more thorough analysis of the MCD of each chromophore. However, as MCD spectroscopy generally provides a more diagnostically useful spectrum than UV–visible absorption spectroscopy for use in empirical comparisons between purified metalloproteins and potential model systems designed as mimics of particular active sites, these spectra do provide a characteristic spectroscopic signature of each protein.

Transferrin and conalbumin

A single, positive MCD transition of intermediate intensity ($\Delta\epsilon = 1.8$ M^{-1} cm^{-1} T^{-1}) at 330 nm is observed for both transferrin and conalbumin when ferric iron is bound. As no change in intensity is observed for the transferrin sample over a 60° temperature range (−30 to +30 °C), the 330 nm band was suggested to be a MCD *B* term [102]. As noted by the authors, definitive assignment would require examination over a wider temperature range. It is interesting to note that the most intense feature in the UV–visible absorption spectrum of ferric transferrin, which is at 465 nm, does not exhibit MCD intensity under the conditions employed. The major MCD feature at 330 nm is suggested by the authors to be characteristic of high-spin ferric iron in an octahedral ligand environment of oxygen and nitrogen donors.

Hemerythrin

Given the extensive amount of spectroscopic work that has been carried out to date on the dinuclear iron site in hemerythrin (see refs. 162–165), it is surprising that the only MCD study is that by Ulmer et al. [102]. They observed an entirely positive MCD spectrum at room temperature for oxy-hemerythrin over the 300–600 nm range; three major features of intermediate intensity ($\Delta\epsilon = 1.4$ M^{-1} cm^{-1} T^{-1}) were seen at 330, 380 and 503 nm. Although oxy- and met-hemerythrin have generally similar electronic and structural properties [162,164], the MCD spectrum of met-hemerythrin is distinctively different from that just described for the oxygenated protein. Two major MCD features of intermediate ($\Delta\epsilon = 2.5$–3.0 M^{-1} cm^{-1} T^{-1}) intensity and opposite sign are observed at 350 and 438 nm (negative and positive signs, respectively). As discussed above, however, examination over a wide range of temperature and in the near-IR [163] should be carried out to more thoroughly characterize the electronic structures of these two protein states. In addition, numerous other oxidation state and ligand-bound derivatives are known including a semi-met (half oxidized) [166] form.

Protocatechuate 3,4-dioxygenase

Included in a general survey of the physical properties of protocatechuate 3,4-dioxygenese from *Pseudomonas putida*, Bull and Ballou [161] reported the room temperature MCD spectra of the enzyme in its native, substrate-bound and product-bound forms. As is generally the case, the MCD spectra are appreciably more detailed than the corresponding UV–visible absorption spectra. Both the native and substrate-bound enzyme states exhibit similar MCD spectra between 300 and 600 nm featuring two positive, weak ($\Delta\epsilon_M \sim$ 0.2–0.7 M^{-1} cm^{-1} T^{-1}) bands (ca. 335 and ca. 510 nm) and one negative band at about 410 nm of even weaker intensity. However, an additional broad and weak band centered at 750 nm is observed in the substrate complex. Only two broad, positive bands of comparable intensity are observed in the product complex (ca. 355 and ca. 520 nm). Very little is known about the active site structure of protocatechuate 3,4-dioxygenase except that there appears to be a tyrosinate ligand as detected in several laboratories using resonance Raman spectroscopy [167]. Consequently, the MCD spectra described above will at this point primarily serve as diagnostic fingerprints for inorganic chemists attempting to mimic the active sites of non-heme iron enzymes.

ACKNOWLEDGEMENTS

D.M.D. is grateful for the kind hospitality of Ed Solomon and his group during a leave at MIT and Stanford when much of this article was written. During this time D.M.D. had many useful discussions of MCD with Ed Solomon, Mark Allendorf and Richard Reem. J.H.D. wishes to express his great appreciation to Ed Bunnenberg for introducing him to the field of MCD spectroscopy and for continuing support and encouragement. We also wish to thank Ed Svastits for his assistance during the preparation of this article. Philip Stephens' advice and help on many occasions is also much appreciated by both authors. D.M.D. has been supported by the NIH (GM 27659) and by the donors of the Petroleum Research Fund administered by the American Chemical Society. J.H.D. is a Camille and Henry Dreyfus Teacher-Scholar (1982–1987), an Alfred P. Sloan Foundation Research Fellow (1983–1985) and a recipient of a National Institutes of Health Research Career Development Award (1983–1988); MCD studies in his laboratory are supported by the NIH (GM26730).

Note added in proof

A recent important paper by Thomson and coworkers [168] has substantially clarified the nature of the copper sites in cyctochrome *c* oxidase. Low temperature MCD spectra and magnetization measurements permitted the

MCD spectrum of oxidized Cu_A (the magnetically isolated, EPR detectable copper) to be resolved. The key results of this work are: (1) $Cu_A(II)$ is a d^9 ion with one, perhaps two, coordinated thiolates; (2) however, $Cu_A(II)$ is not a typical blue copper center, based on comparisons of the low-temperature MCD of azurin and $Cu_A(II)$; (3) the 830 nm absorption band in resting oxidase can be almost completely assigned to $Cu_A(II)$; (4) $Cu_B(II)$ (also designated Cu_{a_3}) and heme a_3^{3+} make almost no contribution to the MCD spectrum of resting oxidase. This paper also reports the 4.2 K MCD spectrum of azurin, which is better resolved and much more intense than the room temperature spectrum reported earlier [38], as expected.

MCD spectroscopy has been used to further characterize Cd,Zn-metallothioneins [169]. Metallothioneins isolated from rat liver and the crab *Scylla serrata* have very similar cadmium-binding sites, according to the MCD data. Further, the metallothionein MCD spectra are most similar to the MCD spectra displayed by model complexes with a near-tetrahedral geometry around cadmium [170]. MCD spectroscopy also established that the apo-metallothioneins prepared at low pH can be reconstituted to provide essentially unaltered cadmium sites.

Several papers reporting MCD experiments on iron–sulfur proteins and models have recently appeared. Nakamura and coworkers prepared a series of models for oxidized rubredoxin in which they complexed the ferric iron to cysteine-containing di-, tri- and tetra-peptides [171]. The complexes were characterized by UV-visible absorption, CD, MCD and EPR spectroscopy and compared to properties of the oxidized protein. The relatively close spectral correspondence between the models and oxidized rubredoxin make it likely that the models were indeed tetrahedral $Fe(SR)_4$ complexes. Unfortunately only tabulated MCD data were reported. Furthermore, the complexes decomposed with half-lives of from 1–25 min at 33°C. Nonetheless, the tabulated MCD parameters of the model complexes, especially the ones with Cys-Pro-Leu-Cys (one of the natural sequences found in rubredoxin for the chelating cysteines) and Cys-Ala-Ala-Cys, match those of oxidized rubredoxin better than do those of previous model systems (see Section F(i)).

The Rieske iron–sulfur protein from *Thermus thermophilus* has been purified to electrophoretic homogeneity and extensively characterized by UV-visible, CD, MCD, EPR and Mössbauer spectroscopy [172]. The MCD spectra of the oxidized and reduced protein are different from those of any other known iron–sulfur cluster. On this basis, together with the other spectroscopic data, the authors proposed that the protein has an $Fe_2S_2X_4$ prosthetic group where at most two of the four amino acid ligands (X) are derived from cysteine. They further suggest that a similar prosthetic group structure may be present in several NADH-dependent dioxygenases.

Two ferredoxins from *Desulfovibrio africanus* have recently been char-

acterized by ultra-low-temperature MCD spectroscopy [173]. Both proteins display similar MCD spectra in their oxidized and reduced states. Furthermore, the MCD spectral properties of both proteins are quite similar to those of *Clostridium pasteurianum* ferredoxin in either oxidation state (see Section F(ii)). Importantly, the oxidized, diamagnetic states of both proteins are free from any paramagnetic impurities (such as those present in the *Clostridial* protein [114]) and therefore the MCD spectra are temperature-independent. In addition the reduced, paramagnetic states displayed superimposable magnetization curves at all wavelengths corresponding to the major MCD bands. It was suggested that the observation of superimposable magnetization curves is a critical criterion of sample homogeneity.

In the previous discussion of aconitase [Section F(iv)], we suggested that low-temperature MCD would prove extremely useful in characterizing the prosthetic group of aconitase. This has, indeed, proved to be the case, as demonstrated in a recent and elegant study from the Thomson laboratory [174]. The low-temperature MCD properties of oxidized and dithionite-reduced aconitase in the absence of added iron clearly show that the prosthetic group is a three-iron center. *Azotobacter crooccosum* ferredoxin I was also examined in its oxidized state and found to be a three-iron cluster. Subtle distinctions, primarily in the 500–800 nm region, were found among the several known three-iron cluster proteins suggesting that three classes may exist; aconitase, *A. crooccocum* ferredoxin I and *D. gigas* ferredoxin II (see Section F(iv) and Fig. 23) are representative examples of each group. Both oxidation states of aconitase exhibit MCD bands in the near-IR region. In contrast to all three oxidation states of the four-iron clusters, which only have positive MCD features in the near-IR, oxidized aconitase displays both positive and negative peaks in the near-IR. Reduced aconitase only has positive features in this region. Thus, as discussed in Section F(v), MCD spectroscopy can clearly distinguish each type of known iron–sulfur center, provided both available oxidation states of a given cluster are examined. Additional important conclusions reached in this aconitase study include: (1) in the presence of added iron, aconitase converts into a four-iron cluster and achieves maximal activity; (2) magnetization studies of oxidized and reduced aconitase are consistent with $S = 1/2$ and $S = 2$ ground states, respectively; and (3) in dithionite-treated preparations having MCD spectra characteristic of reduced three-iron centers, as much as 60% maximal enzymatic activity is found, which suggests that the three-iron form of aconitase may have partial catalytic activity.

Finally, low-temperature MCD studies of the nitrogenase iron–molybdenum cofactor and of a mutant MoFe protein lacking the cofactor have been reported [175]. Robinson et al. [175] confirmed their earlier assignments for the MCD spectra of the intact MoFe protein (see Section F(vi)). In

particular, the low-temperature MCD spectrum of the reduced MoFe protein [157] is dominated by the iron–molybdenum cofactor; the thionine-oxidized MoFe protein displays a low-temperature MCD spectrum essentially devoid of spectral features assignable to the cofactor.

We have recently completed a review on the applications of MCD spectroscopy to the study of iron porphyrins and heme proteins [176].

REFERENCES

1 P.J. Stephens, in P. Day (Ed.), Electronic States of Inorganic Compounds. New Experimental Techniques, D. Reichel, Dordrecht, 1977, pp. 141–156.
2 P.J. Stephens, Ann. Rev. Phys. Chem., 25 (1974) 201–232.
3 P.J. Stephens, Adv. Chem. Phys., 35 (1976) 197–264.
4 S.B. Piepho and P.N. Schatz, Group Theory in Spectroscopy with Applications to Magnetic Circular Dichroism, Wiley, New York, 1983.
5 A.D. Buckingham, P.J. Stephens, Ann. Rev. Phys. Chem., 17 (1966) 339–432.
6 P.N. Schatz and A.J. McCaffery, Q. Rev., Chem. Soc., 23 (1969) 552–584.
7 A.J. McCaffery, Essays Chem., 7 (1977) 13–29.
8 B. Briat, in P. Day (Ed.), Electronic States of Inorganic Compounds. New Experimental Techniques, D. Reichel, Dordrecht, 1977, pp. 177–221.
9 B. Holmquist and B.L. Vallee, Methods Enzymol., 49 (1978) 149–179.
10 B.L. Vallee and B. Holmquist, Adv. Inorg. Biochem., 2 (1980) 27–74.
11 J.C. Sutherland and B. Holmquist, Ann. Rev. Biophys. Bioeng., 9 (1980) 293–326.
12 T.A. Kaden, Metal Ions Biol. Sys., 4 (1974) 1.
13 A.J. McCaffery, P.J. Stephens and P.N. Schatz, Inorg. Chem., 6 (1967) 1614–1625.
14 S.B. Piepho, in J.C. Donini (Ed.), Recent Advances in Group Theory and Their Application to Spectroscopy, Plenum, New York, 1979, pp. 405–491.
15 P.N. Schatz and A.J. McCaffery, Q. Rev., Chem. Soc., 24 (1970) 329.
16 J.G. Foss and M.E. McCarville, J. Chem. Phys., 44 (1966) 4350–4351.
17 B. Briat, D.A. Schooley, R. Records, E. Bunnenberg, C. Djerassi and F. Vogel, J. Am. Chem. Soc., 90 (1968) 4691–4697.
18 J. Michl, J. Am. Chem. Soc., 100 (1978) 6801–6811 and subsequent papers in that issue.
19 H. Isci and W.R. Mason, Inorg. Chem., 14 (1975) 905–912.
20 J.G. Foss and M.E. McCarville, J. Am. Chem. Soc., 89 (1966) 30–32.
21 H. Weiler-Feilchenfeld, R.E. Linder, G. Barth, E. Bunnenberg and C. Djerassi, Theor. Chim. Acta, 46 (1977) 79–88.
22 P.N. Schatz, R.L. Mowery and E.R. Krausz, Mol. Phys., 35 (1978) 1535–1557.
23 P.J. Stephens, J. Chem. Phys., 52 (1970) 3489–3516.
24 H. Katô, Mol. Phys., 24 (1972) 81–97.
25 Y. Sugiura, Y. Hirayama, H. Tanaka and K. Ishizu, J. Am. Chem. Soc., 97 (1975) 5577–5581.
26 J.C. Rival and B. Briat, Mol. Phys., 27 (1974) 1081–1108.
27 S.R. Desjardins, K.W. Penfield, S.L. Cohen, R.L. Musselman and E.I. Solomon, J. Am. Chem. Soc., 105 (1983) 4590–4603.
28 U. Weser, E. Bunnenberg, R. Cammack, C. Djerassi, L. Flohe, G. Thomas and W. Voelter, Biochim. Biophys. Acta, 243 (1971) 203–213.
29 G. Rotilio, L. Calabrese and J.E. Coleman, J. Biol. Chem., 248 (1973) 3855–3859.
30 M. Gabriel, G. Godbillon, D. Larcher, H. Rinnert and C. Thirion, Experientia, 28 (1972) 1019–1020.

31 W. Mori, O. Yamauchi, Y. Nakao and A. Nakahara, Biochem. Biophys. Res. Commun., 66 (1975) 725–730.
32 R.S. Himmelwright, N.C. Eickman, C.D. Lubien and E.I. Solomon, J. Am. Chem. Soc., 102 (1980) 5378–5388.
33 E.I. Solomon, D.M. Dooley, R.H. Wang, H.B. Gray, M. Cerdonio, F. Mogno and G.L. Romani, J. Am. Chem. Soc., 98 (1976) 1029–1031.
34 D.M. Dooley, R.A. Scott, J. Ellinghaus, E.I. Solomon and H.B. Gray, Proc. Nat. Acad. Sci. U.S.A., 75 (1978) 3019–3022.
35 E.I. Solomon, J.W. Hare and H.B. Gray, Proc. Nat. Acad. Sci. U.S.A., 73 (1976) 1389–1393.
36 D.M. Dooley, J. Rawlings, J.H. Dawson, P.J. Stephens, L.-E. Andréasson, B.G. Malmström and H.B. Gray, J. Am. Chem. Soc., 101 (1979) 5038–5046.
37 J.H. Dawson, D.M. Dooley, R. Clark, P.J. Stephens and H.B. Gray, J. Am. Chem. Soc., 101 (1979) 5046–5053.
38 E.I. Solomon, J.W. Hare, D.M. Dooley, J.H. Dawson, P.J. Stephens and H.B. Gray, J. Am. Chem. Soc., 102 (1980) 168–178.
39 D.M. Dooley, J.H. Dawson, P.J. Stephens and H.B. Gray, Biochemistry, 20 (1981) 2024–2028.
40 E.I. Solomon and H.B. Gray, in T. Spiro (Ed.), Copper Proteins, Wiley, NY, 1981, pp. 1–39.
41 E.T. Adman, R.E. Stenkamp, L.C. Sieker and L.H. Jensen, J. Mol. Biol., 123 (1978) 35–47.
42 P.M. Colman, H.C. Freeman, J.M. Guss, M. Murata, V.A. Norris, J.A.M. Ramshaw and M.P. Venkatappa, Nature (London), 272 (1978) 219–324.
43 C. Bergman, E.-K. Gandvik, P.O. Nyman and L. Strid, Biochem. Biophys. Res. Commun., 77 (1977) 1052–1059.
44 M. Hervé, A. Garnier, L. Tosi and M. Steinburk, Eur. J. Biochem., 116 (1981) 177–183.
45 D.G. Eglinton, M.K. Johnson, A.J. Thomson, P.E. Gooding and C. Greenwood, Biochem. J., 191 (1980) 319–331.
46 A.J. Thomson, M.K. Johnson, C. Greenwood and P.E. Gooding, Biochem. J., 193 (1981) 687–697.
47 M.F. Tweedle, L.J. Wilson, L. Garcia-Iniquez, G. Babcock and G. Palmer, J. Biol. Chem., 253 (1978) 8068–8071.
48 K.J. Ellis, Inorg. Perspec. Biol. Med., 1 (1975) 101–135.
49 B. Holmquist, Adv. Inorg. Biochem., 2 (1980) 75–93.
50 C. Görller-Walrand and J. Godemont, J. Chem. Phys., 66 (1977) 48–50.
51 C. Görller-Walrand and J. Godemont, J. Chem. Phys., 67 (1977) 3655–3658.
52 C. Görller-Walrand, H. Peeters, Y. Beyens, N. De Mortié-Neyt and M. Behets, Nouv. J. Chim., 4 (1980) 715–722.
53 J.P. Sipe, III and R.B. Martin, J. Inorg. Nucl. Chem., 36 (1974) 2122–2124.
54 H. Donato and R.B. Martin, Biochemistry, 13 (1974) 4575–4579.
55 B. Holmquist and W.D. Horrocks, Fed. Proc., 34 (1975) 594.
56 R.B. Homer and B.D. Mortimer, FEBS Lett., 87 (1978) 69–72.
57 C.E. Richardson and W.D. Behnke, Biochim. Biophys. Acta, 534 (1984) 267–274.
58 R.G. Denning and J.A. Spencer, Symp. Faraday Soc., 3 (1969) 84–91.
59 J.A. Lomenzo, B.D. Bird, G.A. Osborne and P.J. Stephens, Chem. Phys. Lett., 9 (1971) 332–335.
60 M.J. Harding and B. Briat, Mol. Phys., 25 (1973) 745–776.
61 A.J. McCaffery, P.J. Stephens and P.N. Schatz, Inorg. Chem., 6 (1976) 1614–1625.

62 H. Katô and K. Akimoto, J. Am. Chem. Soc., 96 (1974) 1351–1357.
63 T.A. Kaden, B. Holmquist and B.L. Vallee, Inorg. Chem., 13 (1974) 2585–2590.
64 S.A. Latt and B.L. Vallee, Biochemistry, 10 (1971) 4263–4270.
65 T.A. Kaden, B. Holmquist and B.L. Vallee, Biochem. Biophys. Res. Commun., 46 (1972) 1654–1659.
66 J.E. Coleman and R.V. Coleman, J. Biol. Chem., 247 (1972) 4718–4728.
67 B. Holmquist, T.A. Kaden and B.L. Vallee, Biochemistry, 14 (1975) 1454–1461.
68 K.F. Geoghegan, B. Holmquist, C.A. Spilburg and B.L. Vallee, Biochemistry, 22 (1983) 1847–1852.
69 K. Breddam, T. Bazzone, B. Holmquist and B.L. Vallee, Biochemistry, 18 (1979) 1563–1570.
70 W.D. Behnke and B.L. Vallee, Proc. Nat. Acad. Sci. U.S.A., 69 (1972) 2442–2445.
71 B. Holmquist, Biochemistry, 16 (1977) 4591–4594.
72 F.F. Morpeth and V. Massey, Biochemistry, 21 (1982) 1381–1323.
73 B.L. Vallee, D.L. Drum and F.S. Kennedy, in R.G. Thurman (Ed.), Alcohol and Aldehyde Metabolizing Systems, Vol. 1, Academic Press, NY, 1974, p. 55.
74 R.A. Anderson, F.S. Kennedy and B.L. Vallee, Biochemistry, 15 (1976) 3710–3716.
75 R.A. Anderson and B.L. Vallee, Biochemistry, 16 (1977) 4388–4392.
76 C.-Y. Kwan, K. Erhard and R.C. Davis, J. Biol. Chem., 250 (1975) 5951–5959.
77 C.E. Richardson and W.D. Behnke, J. Mol. Biol., 102 (1976) 441–451.
78 I. Bertini, G. Canti, C. Luchinat and A. Scozzafava, J. Am. Chem. Soc., 100 (1978) 4873–4877.
79 K.K. Kannan, B. Nostrand, K. Fridborg, S. Lövgren, A. Ohlsson and M. Petef, Proc. Nat. Acad. Sci. U.S.A., 72 (1978) 51–55.
80 J.E. Coleman and J.F. Chlebowski, Adv. Inorg. Biochem., 1 (1979) 1–66.
81 J.S. Taylor, C.Y. Lau, M.L. Applebury and J.E. Coleman, J. Biol. Chem., 248 (1973) 6216–6220.
82 S. Suzuki, W. Mori, J. Kino, Y. Nakao and A. Nakahara, J. Biochem. (Tokyo), 88 (1980) 1207–1209.
83 B. Mondovi and F. Finazzi-Agro, Adv. Exp. Biol. Med., 148 (1982) 141–153.
84 S. Suzuki, J. Kino, M. Kimura, W. Mori and A. Nakahara, Inorg. Chim. Acta, 66 (1982) 41–47.
85 S. Suzuki, J. Kino and A. Nakahara, Bull. Chem. Soc. Jpn., 55 (1982) 212–217.
86 E.I. Solomon, in T.G. Spiro (Ed.), Copper Proteins, Wiley, New York, 1981, pp. 41–108.
87 D.R. McMillin, R.A. Holwerda and H.B. Gray, Proc. Nat. Acad. Sci. U.S.A., 71 (1974) 1338–1341.
88 D.R. McMillin, R.C. Rosenberg and H.B. Gray, Proc. Nat. Acad. Sci. U.S.A., 71 (1974) 4760–4762.
89 E.I. Solomon, J. Rawlings, D.R. McMillin, P.J. Stephens and H.B. Gray, J. Am. Chem. Soc., 98 (1976) 8046–8048.
90 S.W. May and J.-Y. Kuo, Biochemistry, 17 (1978) 3333–3338.
91 G.S. Baldwin, A. Galdes, H.A.O. Hill, S.G. Waley and E.P. Abraham, J. Inorg. Biochem., 13 (1980) 189–204.
92 M. Vasák, J. Am. Chem. Soc., 102 (1980) 3953–3955.
93 M. Vasák, J.H.R. Kagi, B. Holmquist and B.L. Vallee, Biochemistry, 20 (1981) 6659–6664.
94 A.Y.C. Law and M.J. Stillman, Biochem. Biophys. Res. Commun., 102 (1981) 397–402.
95 G.A. Carson, P.A.W. Dean and M.J. Stillman, Inorg. Chim. Acta, 56 (1981) 59–71.
96 J.A. Szymanska and M.J. Stillman, Biochem. Biophys. Res. Commun., 108 (1982) 919–925.

97 B. Holmquist and B.L. Vallee, Proc. Nat. Acad. Sci. U.S.A., 76 (1979) 6216–6220.
98 K.F. Geoghegan, A. Galdes, R.A. Martinelli, B. Holmquist, D.A. Auld and B.L. Vallee, Biochemistry, 22 (1983) 2255–2262.
99 T.G. Spiro (Ed.), Iron–Sulfur Proteins, Wiley, New York, 1982.
100 C.D. Stout, D. Ghosh, V. Pattabhi and A. Robbins, J. Biol. Chem., 255 (1980) 1797–1800.
101 D.I. Marlborough, D.O. Hall and R. Cammack, Biochem. Biophys. Res. Commun., 35 (1969) 410–413.
102 D.D. Ulmer, B. Holmquist and B.L. Vallee, Biochem. Biophys. Res. Commun., 51 (1973) 1054–1061.
103 W.A. Eaton and W. Lovenberg, in W. Lovenberg (Ed.), Iron–Sulfur Proteins, Academic Press, NY, 1973, pp. 131–162.
104 J.C. Rivoal, B. Briat, R. Cammack, D.O. Hall, K.K. Rao, I.N. Douglas and A.J. Thomson, Biochim. Biophys. Acta, 493 (1977) 122–131.
105 M.K. Johnson, A.E. Robinson and A.J. Thomson, in T.G. Spiro (Ed.), Iron–Sulfur Proteins, Wiley, N.Y., 1982, pp. 368–406.
106 T. Muraoka, T. Nozawa and M. Hatano, Chem. Lett., (1976) 1373–1378.
107 T. Muraoka, T. Nozawa and M. Hatano, Bioinorg. Chem., 8 (1978) 45–59.
108 Y. Sugiura, K. Ishizu, T. Kimura and H. Tanaka, Bioinorg. Chem., 4 (1975) 291.
109 R.W. Lane, J.A. Ibers, R.B. Franks, G.C. Papaefthymiou and R.H. Holm, J. Am. Chem. Soc., 99 (1977) 84–98.
110 M. Millar, J.F. Lee, S.A. Koch and R. Kikar, Inorg. Chem., 21 (1982) 4106–4108.
111 J.C. Sutherland, I. Salmeen, A.S.K. Sun and M.P. Klein, Biochim. Biophys. Acta, 263 (1972) 550–554.
112 A.J. Thomson, R. Cammack, D.O. Hall, K.K. Rao, B. Briat, J.C. Rivoal and J. Badoz, Biochim. Biophys. Acta, 493 (1977) 132–141.
113 P.J. Stephens, A.J. Thomson, J.B.R. Dunn, T.A. Keiderling, J. Rawlings, K.K. Rao and D.O. Hall, Biochemistry, 17 (1978) 4770–4778.
114 M.K. Johnson, A.J. Thomson, A.E. Robinson, K.K. Rao and D.O. Hall, Biochim. Biophys. Acta, 667 (1981) 433–451.
115 E. Bayer, A. Bacher, P. Krauss, W. Voelter, G. Barth, E. Bunnenberg and C. Djerassi, Eur. J. Biochem., 22 (1971) 580–584.
116 D.M. Kurtz, R.H. Holm and G.B. Wong, J. Am. Chem. Soc., 100 (1978) 6777–6779.
117 G.B. Wong, D.M. Kurtz, R.H. Holm, L.E. Mortenson and R.G. Upchurch, J. Am. Chem. Soc., 101 (1979) 3078–3090.
118 G. Palmer, W.R. Dunham, J.A. Fee, R.H. Sands, T. Iizuka and T. Yonetani, Biochim. Biophys. Acta, 245 (1971) 201–207.
119 R.C. Bray, A.J. Chisholm, L.I. Hart, L.S. Meriwether and D.C. Watts, in E.C. Slater (Ed.), Flavins and Flavoproteins, Elsevier, New York, 1966, pp. 117–132.
120 J.J. Mayerle, R.B. Frankel, R.H. Holm, J.A. Ibers, W.D. Phillips and F.F. Weiher, Proc. Nat. Acad. Sci. U.S.A., 70 (1973) 2429–2433.
121 J.J. Mayerle, S.E. Denmark, B.V. DePamphilis, J.A. Ibers and R.H. Holm, J. Am. Chem. Soc., 97 (1975) 1032–1045.
122 T. Kimura, A. Tasaki and H. Watari, J. Biol. Chem., 245 (1970) 4450–4452.
123 W.H. Orme-Johnson, in G.L. Eichhorn (Ed.), Inorganic Biochemistry, Elsevier, New York, 1973, pp. 710–744.
124 C.W. Carter, in W. Lovenberg (Ed.), Iron–Sulfur Proteins, Vol. III, Academic Press, New York, 1977, pp. 157–204.
125 J.M. Berg and R.H. Holm, in T.G. Spiro (Ed.), Iron–Sulfur Proteins, Wiley, New York, 1982, pp. 1–66.

126 R. Mason and J.A. Zubieta, Angew. Chem. Int. Ed. Engl., 12 (1973) 390–395.
127 P.J. Stephens, A.J. Thomson, T.A. Keiderling, J. Rawlings, K.K. Rao and D.O. Hall, Proc. Nat. Acad. Sci. U.S.A., 75 (1978) 5273–5275.
128 W.H. Orme-Johnson and N.R. Orme-Johnson, in T.G. Spiro (Ed.), Iron–Sulfur Proteins, Wiley, New York, 1982, pp. 67–96.
129 B.C. Antanaitis and T.H. Moss, Biochim. Biophys. Acta, 405 (1975) 262–279.
130 W.V. Sweeney, A.J. Bearden and J.C. Rabinowitz, Biochem. Biophys. Res. Commun., 59 (1974) 188–194.
131 G.C. Papaefthymiou, R.B. Foner, E.J. Laskowski and R.H. Holm, J. Phys. (Paris), Colloq-C1, 41 (1980) 493–494.
132 M.H. Emptage, T.A. Kent, B.H. Huynh, J. Rawlings, W.H. Orme-Johnson and E. Münck, J. Biol. Chem., 255 (1980) 1793–1796.
133 D. Ghosh, W. Furey, Jr., S. O'Donnell and C.D. Stout, J. Biol. Chem., 256 (1981) 4185–4192.
134 T.A. Kent, J.-L. Dreyer, M.C. Kennedy, B.H. Huynh, M.H. Emptage, H. Beinert and E. Münck, Proc. Nat. Acad. Sci. U.S.A., 79 (1982) 1096–1100.
135 B.H. Huynh, J.J.G. Moura, I. Moura, T.A. Kent, J. LeGall, A.V. Xavier and E. Münck, J. Biol. Chem., 255 (1980) 3242–3244.
136 E. Münck, in T.G. Spiro (Ed.), Iron–Sulfur Proteins, Wiley, New York, 1982, pp. 147–175.
137 J. LeGall, J.G. Moura, H.D. Peck, Jr. and A.V. Xavier, in T.G. Spiro (Ed.), Iron-Sulfur Proteins. Wiley, New York, 1982, pp. 177–248.
138 C.D. Stout, in T.G. Spiro (Ed.), Iron–Sulfur Proteins, Wiley, New York, 1982, pp. 97–146.
139 B.-K. Teo and R.G. Shulman, in T.G. Spiro (Ed.), Iron–Sulfur Proteins, 1982, Wiley, New York, pp. 343–366.
140 T.G. Spiro, J. Hare, V. Yachandra, A. Gewirth, M.K. Johnson and E. Reinsen, in T.G. Spiro (Ed.), Iron–Sulfur Proteins, Wiley, New York, 1982, pp. 407–423.
141 A.J. Thomson, A.E. Robinson, M.K. Johnson, J.J.G. Moura, I. Moura, A.V. Xavier and J. LeGall, Biochim. Biophys. Acta, 670 (1981) 93–100.
142 A.J. Thomson, A.E. Robinson, M.K. Johnson, R. Cammack, K.K. Rao and D.O. Hall, Biochim. Biophys. Acta, 637 (1981) 423–432.
143 D. Piszkiewicz, O. Gawron and J.C. Sutherland, Biochemistry, 20 (1981) 363–366.
144 W.V. Sweeney, J. Biol. Chem., 256 (1981) 12222–12227.
145 M.K. Johnson, T.G. Spiro and L.E. Mortenson, J. Biol. Chem., 257 (1982) 2447–2452.
146 J.J.G. Moura, I. Moura, T.A. Kent, J.D. Lipscomb, B.H. Huynh, J. LeGall, A.V. Xavier and E. Münck, J. Biol. Chem., 257 (1982) 6259–6267.
147 S.H. Bell, D.P.E. Dickson, C.E. Johnson, R. Cammack, D.O. Hall and K.K. Rao, FEBS Lett., 142 (1982) 143–147.
148 K.S. Hagen and R.H. Holm, J. Am. Chem. Soc., 104 (1982) 5496–5497.
149 M.R. Antonio, B.A. Averill, I. Moura, J.J.G. Moura, W.H. Orme-Johnson, B.-K. Teo and A.V. Xavier, J. Biol. Chem., 257 (1982) 6646–6649.
150 P.J. Stephens, C.E. McKenna, B.E. Smith, H.T. Nguyen, M.-C. McKenna, A.J. Thomson, F. Devlin and J.B. Jones, Proc. Nat. Acad. Sci. U.S.A., 76 (1979) 2585–2589.
151 P.J. Stephens, C.E. McKenna, M.C. McKenna, H.T. Nguyen and F. Devlin, Biochemistry, 20 (1981) 2857–2864.
152 R.W.F. Hardy, F. Bottomley and R.C. Burns (Eds.), Treatise on Dinitrogen Fixation, Wiley, New York, 1979.
153 W.E. Newton and W.H. Orme-Johnson (Eds.), Nitrogen Fixation, University Park Press, Baltimore, 1980.

154 A. Müller and W.E. Newton (Eds.), Nitrogen Fixation: The Chemical–Biochemical–Genetical Interfaces, Plenum, New York, 1981.
155 B.E. Smith and G. Lang, Biochem. J., 137 (1974) 169–180.
156 B.M. Hoffman, R.A. Venters, J.E. Roberts, M. Nelson and W.H. Orme-Johnson, J. Am. Chem. Soc., 104 (1982) 4711–4712.
157 M.K. Johnson, A.J. Thomson, A.E. Robinson and B.E. Smith, Biochim. Biophys. Acta, 671 (1981) 61–70.
158 E. Münck, H. Rhodes, W.H. Orme-Johnson, L.C. Davis, W.J. Brill and V.K. Shah, Biochim. Biophys. Acta, 400 (1975) 32–53.
159 R. Zimmerman, E. Münck, W.J. Brill, V.K. Shah, M.T. Henzl, J. Rawlings and W.H. Orme-Johnson, Biochim. Biophys. Acta, 537 (1978) 185–207.
160 B.H. Huynh, M.T. Henzl, J.A. Christner, R. Zimmerman, W.H. Orme-Johnson and E. Münck, Biochim. Biophys. Acta, 623 (1980) 124–138.
161 C. Bull and D.P. Ballou, J. Biol. Chem., 256 (1981) 12673–12680.
162 J.S. Loehr and T.M. Loehr, Adv. Inorg. Biochem., 1 (1979) 235–252.
163 J.S. Loehr, T.M. Loehr, A.G. Mauk and H.B. Gray, J. Am. Chem. Soc., 102 (1980) 6992–6996.
164 W.T. Elam, E.A. Stern, J.D. McCallum and J. Sanders-Loehr, J. Am. Chem. Soc., 104 (1982) 6369–6373.
165 W.A. Hendrickson, M.S. Co, J.L. Smith, K.O. Hodgson and G.L. Klippenstein, Proc. Nat. Acad. Sci. U.S.A., 79 (1982) 6255–6259.
166 P.C. Harrington, D.J.A. DeWaal and R.G. Wilkins, Arch. Biochem. Biophys., 191 (1978) 444–451.
167 L. Que, Struct. Bonding (Berlin), 40 (1980) 39–72.
168 C. Greenwood, B.C. Hull, D. Barber, D.G. Eglinton, and A.J. Thomson, Biochem. J., 215 (1983) 303–316.
169 A.Y.C. Law, M.G. Sherian, and M.J. Stillman, Biochim. Biophys. Acta, 784 (1984) 53–61.
170 G.K. Carson, P.A.W. Dean, and M.J. Stillman, Inorg. Chim. Acta, 56 (1981) 59–71.
171 M. Nakata, N. Ueyama, T. Terakawa, and A. Nakamura, Bull. Chem. Soc. Jpn., 56 (1983) 3647–3651.
172 J.A. Fee, K.L. Findling, T. Yoshida, R. Hille, G.E. Tarr, D.O. Hearshen, W.R. Dunham, E.P. Day, T.A. Kent and E. Münck, J. Biol. Chem., 259 (1984) 124–133.
173 E.C. Hatchian, R. Cammack, D.S. Patil, A.E. Robinson, A.J.M. Richards, S. George, and A.J. Thomson, Biochim. Biophys. Acta, 784 (1984) 40–47.
174 M.K. Johnson, A.J. Thomson, A.J.M. Richards, J. Peterson, A.E. Robinson, R.R. Ramsay and T.P. Singer, J. Biol. Chem., 259 (1984) 2274–2282.
175 A.E. Robinson, A.J.M. Richards, A.J. Thomson, T.R. Hawkes and B.E. Smith, Biochem. J., 219 (1984) 495–503.
176 J.H. Dawson and D.M. Dooley, in A.B.P. Lever and H.B. Gray (Eds.), Iron Porphyrins, Part III, Benjamin-Cummings, in preparation.